UNIVERSITÉ DU QUÉBEC À MONTRÉAL

IMPACT OF INTERACTIVE VEGETATION PHENOLOGY ON THE SIMULATED PAN-ARCTIC LAND SURFACE STATE

DISSERTATION

PRESENTED

AS PARTIAL REQUIREMENT

FOR MSC DEGREE IN ATMOSPHERIC SCIENCES

BY

BERNARDO STEPHAN TEUFEL

MARCH 2016

UNIVERSITÉ DU QUÉBEC À MONTRÉAL

EFFETS DE L'INCLUSION DE LA PHÉNOLOGIE INTERACTIVE DE LA VÉGÉTATION SUR L'ÉTAT DE SURFACE SIMULÉ DU DOMAINE PANARCTIQUE

MÉMOIRE

PRÉSENTÉ

COMME EXIGENCE PARTIELLE

DE LA MAÎTRISE EN SCIENCES DE L'ATMOSPHÈRE

PAR

BERNARDO STEPHAN TEUFEL

MARS 2016

TABLE OF CONTENTS

LIST OF FIGURES v
RÉSUMÉ vii
ABSTRACT ix
CHAPTER I
INTRODUCTION 1
1.1 Context 1
1.2 Objective and methods 7
CHAPTER II
IMPACT OF INTERACTIVE VEGETATION PHENOLOGY ON THE SIMULATED PAN-ARCTIC LAND SURFACE STATE 11
2.1 Introduction 13
2.2 Methods 16
2.2.1 Model description 16
2.2.2 Experiments 18
2.2.3 Soil properties 21
2.2.4 Spatial distribution of PFTs 22
2.2.5 Validation data 23
2.3 Results 25
2.3.1 Validation 25
2.3.2 Impact of deep soil column 27
2.3.3 Impact of interactive phenology (recent past) 29
2.3.4 Impact of interactive phenology on projected changes 31
2.4 Summary and conclusions 33
FIGURES 37
CHAPTER III

CONCLUSION 49

APPENDIX A
SUPPLEMENTARY FIGURES 53

REFERENCES 61

LIST OF FIGURES

Figure Page

2.1 Number of prescribed organic soil layers : dark blue is used for grid cells with 0 layers, cyan for 1 layer (10 cm), yellow for 2 layers (30 cm) and red for deep organic soils. 37

2.2 Prescribed fractional coverages of plant functional types : (a) needleleaf evergreen trees, (b) needleleaf deciduous trees, (c) broadleaf deciduous trees, (d) crops, (e) grasses, (f) bare soil 38

2.3 Mean PAI [m^2 m^{-2}] for the 1982-1998 period from (a) CLASS26_CTEM/ERA, (b) ISLSCP II. 39

2.4 Mean NPP [kgC m^{-2} yr^{-1}] for the 2000-2010 period from (a) CLASS26_CTEM/ERA, (b) MODIS. 39

2.5 Soil carbon density [kg m^{-2}] from (a) CLASS26_CTEM/ERA for the 1981-1990 period, (b) IGBP, (c) NCSCD. 40

2.6 (a) Mean 1981-1990 active layer thickness [m] of near-surface permafrost, simulated by CLASS26_CTEM/ERA. (b) Observed permafrost extent: magenta, continuous (>90%); blue, discontinuous (50-90%); green, sporadic (10-50%); yellow, isolated (<10%) 40

2.7 Comparison between modelled and observed ALT [m] for the 1990-2012 period. Here blue circles are used for CLASS26_CTEM/ERA and green triangles for CLASS26/ERA 41

2.8 (a) Difference (CLASS26_CTEM/ERA - CLASS3_CTEM/ERA) in 1981-2010 annual maximum temperature [K] of the first soil layer. (b) Same, but for annual minimum temperature 42

2.9 (a) Difference (CLASS26_CTEM/ERA - CLASS3_CTEM/ERA) in 1981-2010 annual maximum PAI [m^2 m^{-2}]. (b) Same, but for average root zone moisture availability (adimensional : equal to zero at the wilting point and below, equal to one at field capacity and above). 42

2.10 (a) Difference (CLASS26_CTEM/ERA - CLASS26/ERA) in 1981-2010 annual maximum PAI [m^2 m^{-2}]. (b) Same, but for PAI during June. 43

2.11 (a) Difference (CLASS26_CTEM/ERA - CLASS26/ERA) in 1981-2010 average evapotranspiration [mm day^{-1}]. (b) Same, but for average runoff. .. 43

2.12 (a) Difference (CLASS26_CTEM/ERA - CLASS26/ERA) in 1981-2010 summer temperature [K] of the first soil layer. (b) Same, but for ALT [m]. 44

2.13 Projected changes (2071-2100 average minus 1981-2010 average) in driving data : (a) air temperature [K], (b) air specific humidity [kg kg^{-1}], (c) precipitation [mm day^{-1}], (d) incoming shortwave radiation [W m^{-2}]..... 45

2.14 Projected changes (2071-2100 minus 1981-2010) in : (a,b) spring PAI [m^2 m^{-2}], (c,d) spring ET [mm day^{-1}], (e,f) ALT [m], from CLASS26_CTEM/CRCM in the first column (a,c,e), and from CLASS26/CRCM in the second column (b,d,f). Grey areas in (e,f) represent regions where permafrost in the top 5 meters of soil degraded completely by 2071-2100..... 46

2.15 Differences (CLASS26_CTEM/CRCM - CLASS26/CRCM) in ALT [m] for the (a) 1981-2010 period, (b) 2011-2040, (c) 2041-2070, (d) 2071-2100. ... 47

A.1 (a) Difference (CLASS26_CTEM/ERA - CLASS3_CTEM/ERA) in 1981-2010 winter (DJF) temperature [K] of the first soil layer. (b) Same, but for spring (MAM). (c) Same, but for summer (JJA). (d) Same, but for fall (SON). 54

A.2 (a) Difference (CLASS26_CTEM/ERA - CLASS26/ERA) in 1981-2010 winter (DJF) PAI [m^2 m^{-2}]. (b) Same, but for spring (MAM). (c) Same, but for summer (JJA). (d) Same, but for fall (SON). 55

A.3 (a) Difference (CLASS26_CTEM/ERA - CLASS26/ERA) in 1981-2010 winter (DJF) evapotranspiration [mm day^{-1}]. (b) Same, but for spring (MAM). (c) Same, but for summer (JJA). (d) Same, but for fall (SON). 56

A.4 (a) Difference (CLASS26_CTEM/ERA - CLASS26/ERA) in 1981-2010 winter (DJF) temperature [K] of the first soil layer. (b) Same, but for spring (MAM). (c) Same, but for summer (JJA). (d) Same, but for fall (SON). 57

A.5 (a) Projected changes (2071-2100 minus 1981-2010) in winter (DJF) driving air temperature [K]. (b) Same, but for spring (MAM). (c) Same, but for summer (JJA). (d) Same, but for fall (SON). 58

A.6 (a) Projected changes (2071-2100 minus 1981-2010) in winter (DJF) driving precipitation [mm day^{-1}]. (b) Same, but for spring (MAM). (c) Same, but for summer (JJA). (d) Same, but for fall (SON). 59

RÉSUMÉ

Dans la région panarctique, la surface terrestre subit des changements rapides causés par le réchauffement climatique. Le pergélisol près de la surface devrait se dégrader de manière importante au cours du 21e siècle, provoquant des rétroactions sur le climat mondial et les cycles de l'eau à l'échelle régionale. La réponse de la végétation au réchauffement climatique et à l'augmentation des concentrations atmosphériques de CO2 va influencer l'ampleur de ces rétroactions. Dans cette étude, l'impact de la phénologie interactive sur l'état de la surface terrestre est évalué en comparant deux simulations du schéma canadien de surface (CLASS) — une avec phénologie interactive, modélisée en utilisant le modèle canadien des écosystèmes terrestres (CTEM), et l'autre avec phénologie prescrite. Ces simulations sont réalisées pour la période de 1979 à 2012, en utilisant le forçage atmosphérique de la réanalyse ERA-Interim. Les valeurs simulées de l'indice de surface foliaire, la productivité primaire, l'étendue du pergélisol et l'épaisseur de la couche active sont comparées aux observations disponibles. Les résultats suggèrent que les deux simulations capturent la distribution générale de la végétation et du pergélisol, bien que certaines erreurs demeurent. Des différences significatives dans l'évapotranspiration sont observées entre les deux simulations, conduisant à des différences dans le ruissellement, la température du sol et l'épaisseur de la couche active. Pour évaluer l'impact de la phénologie interactive sur les changements prévus dans l'état de la surface terrestre, deux autres simulations sont comparées, l'une avec CLASS et l'autre avec CLASS couplé à CTEM, en utilisant le forçage atmosphérique d'une simulation transitoire du modèle régional canadien du climat (MRCC5) pour le scénario RCP8.5. Ces deux simulations montrent une dégradation importante du pergélisol près de la surface, mais la simulation avec phénologie interactive montre une perte légèrement plus rapide du pergélisol, pointant vers une rétroaction positive de la végétation sur la température du sol.

Mots-clés: modèle dynamique de la végétation, pergélisol, épaisseur de la couche active, carbone du sol, changement climatique

ABSTRACT

The pan-Arctic land surface is undergoing rapid changes caused by a warming climate. Near-surface permafrost is projected to degrade significantly during the 21st century, resulting in feedbacks to global climate and regional water cycles. Vegetation response to the warming climate and increasing atmospheric CO_2 concentrations will influence the magnitude of these feedbacks. In this study, the impact of interactive phenology on the land surface state is assessed by comparing two simulations of the Canadian Land Surface Scheme (CLASS) - one with interactive phenology, modelled using the Canadian Terrestrial Ecosystem Model (CTEM), and the other with prescribed phenology. These simulations are performed for the 1979-2012 period, using atmospheric forcing from the ECMWF ERA-Interim reanalysis. Simulated plant area index, primary productivity, permafrost and active layer thickness are compared to available observational estimates. Results suggest that both simulations capture the general distribution of vegetation and permafrost, although some biases remain. Significant differences in evapotranspiration are observed between both simulations, leading to differences in runoff, soil temperature and active layer thickness. To assess the impact of interactive phenology on projected changes to the land surface state, two further simulations are compared, one with CLASS and the other with CLASS coupled to CTEM, both driven by atmospheric forcing data from a transient climate change simulation of the 5th generation Canadian Regional Climate Model (CRCM5) for the Representative Concentration Pathway 8.5. Both of these simulations show extensive near-surface permafrost degradation, but the simulation with interactive phenology shows slightly faster permafrost loss, pointing towards a positive feedback of vegetation on soil temperatures.

Keywords : dynamic vegetation model, permafrost, active layer thickness, soil carbon, climate change

CHAPTER I

INTRODUCTION

1.1 Context

Human activities are affecting the Earth's energy budget by changing the atmospheric concentrations of greenhouse gases and aerosols and by changing land surface properties. Carbon dioxide concentrations have increased by 40% since pre-industrial times, primarily from fossil fuel emissions, and have reached levels not seen in the last 800,000 years. The combined effect of these changes has been an uptake of energy by the climate system, resulting in warming of the atmosphere and the ocean, diminishing snow and ice, and rising sea levels (IPCC, 2013).

Climate models, based on the fundamental laws of nature (e.g., energy, mass and momentum conservation), are the primary tools available to investigate the response of the climate system to various forcings and to make projections of future climate. Models are able to reproduce the observed continental-scale surface temperature patterns and trends over many decades, and conclude that continued emissions of greenhouse gases will cause further warming and changes in all components of the climate system (IPCC, 2013).

Regional downscaling methods provide climate information at the smaller scales needed for many climate impact studies, as the horizontal resolution of global models is often too low to resolve features that are important at regional scales (IPCC, 2013). Regional climate models (RCMs) are applied over a limited-area

domain with boundary conditions either from global reanalyses or global climate model output (Laprise, 2008). Downscaling by RCMs adds value mainly in regions with highly variable topography and for various small-scale phenomena (Di Luca *et al.*, 2012; Feser *et al.*, 2011).

One region undergoing rapid changes is the Arctic land surface, which has warmed at a rate of 0.5°C per decade over the past three decades. This rate is significantly higher than the global average warming rate, due to a characteristic of the climate system known as Arctic amplification (IPCC, 2013). Temperatures over the Arctic during the past few decades have been significantly higher than those seen over the past 2000 years (Kaufman *et al.*, 2009).

Arctic amplification has a number of causes, with albedo feedback playing an important role both over the land surface and over the ocean (Serreze and Barry, 2011). Albedo feedback is a positive feedback cycle in which the albedo decreases as highly reflective ice and snow melt, exposing the darker and more absorbing surfaces below and the additional absorbed heat causes further melting. Other positive feedbacks contributing on longer time scales are associated with vegetation changes and thawing permafrost (IPCC, 2013).

Arctic amplification is evident in both the instrumental records and climate model projections through the 21st century (Serreze and Barry, 2011). However, the magnitude of the projected warming strongly depends on assumptions about future greenhouse gas emissions. One possibility is that emissions will continue to increase during the 21st century, which is represented by the Representative Concentration Pathway 8.5 (RCP8.5). Under this scenario, Arctic warming is expected to exceed the global average (2.6 to 4.8°C) by 2.2 to 2.4 times by the end of the 21st century, implying that Arctic temperatures would continue to rise at an average rate of at least 0.5°C per decade (IPCC, 2013).

This ongoing Arctic warming directly affects the cryosphere, as evidenced by decreases of more than 10% per decade in Arctic perennial sea-ice extent since 1979 (IPCC, 2013). Over land, Arctic warming affects the Greenland ice sheet, glaciers and permafrost, which is defined as ground (soil or rock) that remains at or below 0°C for two or more consecutive years. Permafrost was estimated to underlay about 24% of the northern hemisphere land surface during the second half of the 20th century (Zhang *et al.*, 2008).

Given the strong projected warming across the northern high latitudes, substantial near-surface permafrost degradation is expected during the 21st century (Slater and Lawrence, 2013). Permafrost degradation at greater depths occurs much more slowly, but is less relevant to the surface energy and water balance (Delisle, 2007). Following the RCP8.5 scenario, a reduction of around 80% by the end of the 21st century in near-surface permafrost area (areas with permafrost in the top 3.5 m of soil) is projected by the CMIP5 models (Koven *et al.*, 2013; Slater and Lawrence, 2013).

As mentioned previously, the main driver of global warming is the increase in the concentration of greenhouse gases in the atmosphere. However, the concentration of greenhouse gases is also strongly dependant on the global carbon cycle, where soil respiration plays an important role. Soil respiration is the process in which carbon dioxide (CO_2) is produced in soils by roots and soil organisms and subsequently released to the atmosphere. Increased soil respiration with global warming is likely to provide a positive feedback to the greenhouse effect (Raich and Schlesinger, 1992).

Close to 1700 Pg of soil carbon are stored in the northern circumpolar permafrost zone, more than twice as much carbon than in the atmosphere (Tarnocai *et al.*, 2009). This soil carbon accumulated over thousands of years under cold conditions (Schuur *et al.*, 2013). As permafrost thaws, this soil carbon may become

active, leading to emission of greenhouse gases such as methane or carbon dioxide, depending on the amount of water in the soil (Lawrence and Slater, 2005).

There are no direct measurements of soil carbon loss from the permafrost zone at large scales. This is in part due to a scarcity of soil carbon measurements in this region, in combination with an overall difficulty of detecting changes in soil carbon pools due to large soil heterogeneity (Schuur *et al.*, 2013).

According to the latest model projections, around 15% of the simulated permafrost carbon pool is expected to be lost as greenhouse gas emissions by 2100 following the RCP8.5 scenario. Independent estimates from laboratory experiments and assessment by experts agree on 5% to 15% of the permafrost carbon pool being vulnerable under this scenario (Schuur *et al.*, 2015). Future projections of permafrost and soil carbon remain limited given the lack of representation of processes within current models. Even if processes are included, validating them is often problematic due to the scarcity of actual measurements from these remote landscapes. Nevertheless, the release of carbon from permafrost zone soils is likely to influence the pace of climate change in the 21st century and beyond. However, fossil fuel burning is likely to continue to be the main source of carbon emissions and climate forcing (Schuur *et al.*, 2013).

Fire could be an important additional mechanism for releasing permafrost carbon to the atmosphere. Fire frequency and severity are increasing in some parts of the boreal permafrost zone. Thawing and fires could act together to expose and transfer permafrost carbon to the atmosphere very rapidly, especially in ecosystems with organic surface soils (Turetsky *et al.*, 2010).

In addition to affecting the global carbon budget, permafrost thaw alters soil structural and hydrologic properties, with impacts on the spatial extent of lakes and wetlands (Smith *et al.*, 2005) and possibly on the freshwater fluxes to the Arctic

ocean (Lawrence and Slater, 2005). Increasing winter base flow and mean annual stream flow resulting from possible permafrost thawing were reported in northwest Canada (St. Jacques and Sauchyn, 2009). Rising minimum daily flows also have been observed in northern Eurasian rivers (Smith *et al.*, 2007). Changes in the amount of freshwater reaching the Arctic Ocean affect sea-ice formation and may alter the oceanic thermohaline circulation (Arnell, 2005).

An important factor to consider when studying warming and its impacts on permafrost is the role of vegetation changes in future climate. It is known that the distribution of natural vegetation is governed primarily by climate, through precipitation, temperature and radiation (Nemani *et al.*, 2003; Stephenson, 1990). Vegetation variability is driven by climate, through heat/cold stress, drought stress and light. Observations show that temperature is important for forcing vegetation variability in the northern mid/high latitudes while precipitation is important in the tropics and subtropics (Liu *et al.*, 2006).

Specially relevant to permafrost degradation is the fact that vegetation also influences climate, through the biophysical and biogeochemical pathways, where the biogeochemical impacts are via modifying the atmospheric CO_2 concentrations, while the biophysical pathway influences climate through impacts on surface albedo and on the land-atmosphere fluxes of energy, water and momentum. Vegetation growth and expansion tends to lower the surface albedo, resulting in more energy absorption. When snow is present, this change in albedo is even larger (Liu *et al.*, 2006).

The height of vegetation strongly influences surface roughness. Increases in surface roughness are associated with an increase in the efficiency with which sensible heat is transferred from the surface to the atmosphere. Changes in surface roughness can also influence precipitation and large-scale circulation patterns (Richardson *et al.*, 2013).

Observations show that the vegetation feedback on climate is less significant than the climate forcing on vegetation. A strong positive feedback of vegetation on temperature, explaining 10% to 25% of the interannual temperature variance, is observed in the northern mid/high latitudes. The vegetation feedback adds moisture to the atmosphere locally, but the increased moisture might not precipitate locally, resulting in insignificant feedbacks on precipitation, except for some isolated semiarid pockets in the tropics/subtropics (Liu *et al.*, 2006).

The biophysical feedbacks are controlled by mechanisms of regional character and the relative importance of individual feedback mechanisms might differ among regions (Quillet *et al.*, 2010; Wramneby *et al.*, 2010).

Recent warming trends have been associated with earlier onset of vegetation activity in spring, delayed autumn senescence and an overall extension in the length of the active growing season. In high latitude ecosystems, two factors regulate the spring onset: the timing of snowmelt and the temperatures that follow snowmelt. The timing depends on the depth of the winter snowpack and on springtime temperatures. If the snow melts too early, plants might be exposed to cold air temperatures that inhibit development or cause frost damage (Richardson *et al.*, 2013).

Increased atmospheric CO_2 promotes stomatal closure and reduced transpiration (Field *et al.*, 1995). On the other hand, higher temperatures increase the atmospheric demand for water, increasing evapotranspiration (Wramneby *et al.*, 2010). There is potential for substantial feedbacks between vegetation changes and regional water cycles, but the impact of such feedbacks remains uncertain due to limitations in modelling vegetation processes and uncertainties in plant response, ecosystem shifts and land management changes (IPCC, 2013).

A greater availability of CO_2 might increase photosynthesis. Nutrient availability and soil moisture conditions play an important role in this response

(Quillet *et al.*, 2010). The physiological effects of CO_2 on productivity and water-use efficiency decrease with increasing CO_2 concentration, approaching an asymptote at high CO_2 concentrations (Cramer *et al.*, 2001).

Global warming will alter the density of vegetation cover, modifying the physical characteristics of the land surface (Betts *et al.*, 1997). An assessment of changes in plant productivity, inferred from satellite observations between 1982 and 2012 shows that about a third of the pan-Arctic has substantially greened, less than 4% browned, and more than 57% did not change significantly (Xu *et al.*, 2013).

Several studies have calculated the magnitude of the combined effects of vegetation change in the Arctic, including the negative feedbacks of CO_2 sequestration and increased evapotranspiration and the positive feedback of decreased albedo. It is likely that vegetation changes will result in an overall positive feedback to Arctic warming (Pearson *et al.*, 2013; Swann *et al.*, 2010; Wramneby *et al.*, 2010; Zhang *et al.*, 2014), thus favouring near-surface permafrost degradation and its associated impacts on regional hydrology.

1.2 Objective and methods

In order to gain insight into the processes occurring at the land surface in high latitude regions, offline simulations using the Canadian Land Surface Scheme (CLASS) coupled to the Canadian Terrestrial Ecosystem Model (CTEM) are performed over a pan-Arctic domain. These simulations are first performed for the recent past (1979 - 2012), using reanalysis data to drive the models. In a second phase, output from an existing simulation of the 5th generation Canadian Regional Climate Model (CRCM5) is used to drive the models in a climate change (1961 - 2100) scenario, following RCP8.5.

As this is the first time that CLASS and CTEM are used together over a pan-Arctic domain at 0.5 degrees resolution, an assessment of their performance in simulating vegetation, soil carbon and permafrost is necessary. This assessment is performed by comparing model output to observational estimates of several key variables. In order to facilitate this assessment only the basic modules of CTEM are used, which requires the spatial distribution of plant functional types to be prescribed and time-invariant. As the term dynamic vegetation is commonly reserved for models where vegetation can expand horizontally (in addition to vertical growth), the term interactive vegetation phenology is used in this study to represent vegetation that can only grow vertically, following Garnaud *et al.* (2014b).

CLASS and CTEM were originally designed to use a soil column consisting of only 3 vertical layers, extending to a depth of 4.1 m. It was shown by Paquin and Sushama (2014) that such soil depths were insufficient to realistically represent permafrost, a key component of the land surface in the pan-Arctic. As the same study showed that a soil depth of 60 m provided a much better representation of permafrost, it became necessary to use such a deep soil configuration for the present study.

In light of this, a first sensitivity study consists in analyzing the effects of a deep soil configuration on the land surface and on vegetation, which is performed by comparing a simulation of CLASS coupled to CTEM with the original 3 layer configuration to a simulation with a 26 layer configuration, both driven by reanalysis data. This comparison starts by looking at the differences in the thermal regime of the soil, which drives the differences in all other components of the land surface.

The main sensitivity study of this work consists in analyzing the differences between simulations using CLASS coupled to CTEM and simulations using only CLASS. As all these simulations are performed using the deep soil configuration and starting from the same initial conditions, the differences between them originate from the way vegetation is represented within each model.

When CLASS is not coupled to CTEM only the seasonality of vegetation is represented in CLASS, with plant area index (PAI) varying between an annual maximum and minimum PAI, which are prescribed along with all other vegetation related parameters, such as roughness length, rooting depth and canopy mass. When CLASS is coupled to CTEM, vegetation can adapt to climate and PAI as well as all other vegetation parameters are dynamic functions of climate, soil conditions and CO_2 concentrations.

The sensitivity of the simulated land surface to interactive phenology (i.e. CTEM) is first assessed for the simulations driven by reanalysis data, linking the differences between the simulations to differences in PAI and evapotranspiration, which are the main variables affected by introducing CTEM. In a second phase, this sensitivity is also assessed for the simulations driven by CRCM5 output. In this case, the response of the land surface and vegetation to projected climate change is analyzed, and the effect of including interactive phenology on permafrost and other components is assessed.

The objectives of this work can be summarized as follows :

- Assess the quality of the simulations produced by CLASS coupled to CTEM over the pan-Arctic domain, by comparing the simulated vegetation, soil carbon and permafrost to observational estimates.
- Analyze the impact of using a deep soil configuration on the simulated pan-Arctic land surface state and vegetation.
- Analyze the impact of using interactive phenology on the simulated pan-Arctic land surface state, for the recent past and for a climate change scenario.

This work is organized as follows : chapter one presents the context of the research, along with a summary of the methods used and the objectives of this study.

Chapter two presents the main results of this study, in the form of an article to be submitted to a scientific journal, including an introduction in section 2.1, methods in section 2.2, results in section 2.3 and conclusions in section 2.4. Chapter three presents a brief summary of the results and conclusions.

CHAPTER II

IMPACT OF INTERACTIVE VEGETATION PHENOLOGY ON THE SIMULATED PAN-ARCTIC LAND SURFACE STATE

Bernardo Teufel[1,*], Laxmi Sushama[1], Vivek K. Arora[2], Diana Verseghy[1,3]

[1] Centre ESCER (Étude et Simulation du Climat à l'Échelle Régionale), University of Quebec at Montreal, 201-President-Kennedy, Montreal, Canada

[2] Canadian Centre for Climate Modelling and Analysis, Climate Research Division, Environment Canada, University of Victoria, Victoria, Canada

[3] Climate Processes Section, Climate Research Division, Environment Canada, Toronto, Canada

*Corresponding author

Tel : +1 514-987-3000 ext. 2414

Fax : +1 514-987-6853

E-mail : teufel@sca.uqam.ca

(Submitted to Climate Dynamics)

Abstract

The pan-Arctic land surface is undergoing rapid changes caused by a warming climate. Near-surface permafrost is projected to degrade significantly during the 21st century, resulting in feedbacks to global climate and regional water cycles. Vegetation response to the warming climate and increasing atmospheric CO_2 concentrations will influence the magnitude of these feedbacks. In this study, the impact of interactive phenology on the land surface state is assessed by comparing two simulations of the Canadian Land Surface Scheme (CLASS) - one with interactive phenology, modelled using the Canadian Terrestrial Ecosystem Model (CTEM), and the other with prescribed phenology. These simulations are performed for the 1979-2012 period, using atmospheric forcing from the ECMWF ERA-Interim reanalysis. Simulated plant area index, primary productivity, permafrost and active layer thickness are compared to available observational estimates. Results suggest that both simulations capture the general distribution of vegetation and permafrost, although some biases remain. Significant differences in evapotranspiration are observed between both simulations, leading to differences in runoff, soil temperature and active layer thickness. To assess the impact of interactive phenology on projected changes to the land surface state, two further simulations are compared, one with CLASS and the other with CLASS coupled to CTEM, both driven by atmospheric forcing data from a transient climate change simulation of the 5th generation Canadian Regional Climate Model (CRCM5) for the Representative Concentration Pathway 8.5. Both of these simulations show extensive near-surface permafrost degradation, but the simulation with interactive phenology shows slightly faster permafrost loss, pointing towards a positive feedback of vegetation on soil temperatures.

Keywords : dynamic vegetation model, permafrost, active layer thickness, soil carbon, climate change

2.1 Introduction

Over the past three decades the Arctic land surface has warmed at a rate of 0.5°C per decade, which is significantly higher than the global average warming rate (IPCC, 2013). This Arctic amplification has a number of causes, with albedo feedback playing an important role (Serreze and Barry, 2011). Other positive feedbacks contributing on longer time scales are associated with vegetation changes and thawing permafrost (IPCC, 2013). According to the fifth assessment report of the IPCC (2013), Arctic temperatures are projected to continue to rise at an average rate of at least 0.5°C per decade under the Representative Concentration Pathway 8.5 (RCP8.5) scenario.

This ongoing Arctic warming affects permafrost, which is defined as ground that remains at or below 0°C for two or more consecutive years. Permafrost is estimated to underlay about 24% of the northern hemisphere land surface (Zhang *et al.*, 2008). Given the strong projected warming across the northern high latitudes, substantial near-surface permafrost degradation is expected during the 21st century. For instance, following the RCP8.5 scenario, a reduction of around 80% in the near-surface permafrost area (i.e. permafrost in the top 3.5 m below surface) is projected by Koven *et al.* (2013) and Slater and Lawrence (2013), based on models participating in the Coupled Model Intercomparison Project Phase 5 (CMIP5).

This projected degradation of permafrost has important implications for both Arctic and global climates, as close to 1700 Pg of soil carbon are stored in the northern circumpolar permafrost zone (Tarnocai *et al.*, 2009). As permafrost thaws, this soil carbon becomes available for decomposition, potentially leading to the enhanced emission of greenhouse gases (GHG) and thus a positive feedback to global warming (Lawrence and Slater, 2005).

According to the latest model projections, around 15% of the simulated permafrost carbon pool is expected to be lost as GHG emissions by 2100 following

the RCP8.5 scenario. Independent estimates from laboratory experiments and assessment by experts agree on 5% to 15% of the permafrost carbon pool being vulnerable under this scenario (Schuur *et al.*, 2015). Future projections of changes in permafrost and the associated soil carbon remain limited given the lack of representation of processes within current models. Even if relevant processes are included, validating them is often problematic due to the scarcity of actual measurements from these remote landscapes. Nevertheless, the release of carbon from permafrost regions is likely to influence the pace of climate change in the 21st century and beyond, although, fossil fuel burning is likely to continue to be the main source of carbon emissions and climate forcing (Schuur *et al.*, 2013).

An important factor to consider when studying climate warming and its impacts on permafrost is the role of vegetation changes in future climate. It is known that the distribution of natural vegetation is governed primarily by climate, through precipitation, temperature and radiation (Nemani *et al.*, 2003; Stephenson, 1990). Variability in vegetation's structure and areal extent is driven by climate, through heat/cold stress, drought stress and light at sub-annual to decadal timescales. Observations show that temperature is the dominant factor affecting vegetation variability in the northern mid/high latitudes, while precipitation is important in the tropics and subtropics (Liu *et al.*, 2006).

Specially relevant to permafrost degradation is the fact that vegetation also influences climate. For instance, a strong positive feedback of vegetation on temperature, explaining 10% to 25% of the interannual temperature variance, is observed in the northern mid/high latitudes (Liu *et al.*, 2006). The vegetation feedback on climate acts through biophysical and biogeochemical pathways. The biogeochemical pathway impacts are modulated through changes in the atmospheric CO2 concentration and other greenhouse gases, while the biophysical pathway influences climate through impacts on surface albedo and on the land-atmosphere

fluxes of energy, water and momentum. For example, vegetation growth and expansion tends to lower the surface albedo, resulting in more energy absorption. These biophysical feedbacks are controlled by mechanisms operating at regional scales and the relative importance of individual feedback mechanisms might differ among regions (Quillet *et al.*, 2010; Wramneby *et al.*, 2010).

Increased atmospheric CO_2 leads to stomatal closure and reduced transpiration (Field *et al.*, 1995). On the other hand, higher temperatures increase the atmospheric demand for water, increasing evapotranspiration (Wramneby *et al.*, 2010). There is potential for substantial feedbacks between vegetation changes and regional water cycles, but the impact of such feedbacks remains uncertain due to limitations in modelling vegetation processes and uncertainties in plant response, ecosystem shifts and land management changes (IPCC, 2013).

Recent warming trends have been associated with earlier onset of vegetation activity in spring, delayed autumn senescence and an overall extension in the length of the active growing season (Richardson *et al.*, 2013). A higher atmospheric CO_2 concentration also increases photosynthesis trough the CO_2 fertilization effect, but nutrient availability and soil moisture conditions play an important role in this response (Quillet *et al.*, 2010). The physiological effects of CO_2 on productivity and water-use efficiency decrease with increasing CO_2 concentration, approaching an asymptote at high CO_2 concentrations (Cramer *et al.*, 2001).

Several studies (Pearson *et al.*, 2013; Swann *et al.*, 2010; Wramneby *et al.*, 2010; Zhang *et al.*, 2014) have estimated the magnitude of the combined effects of vegetation change in the Arctic, including the negative feedbacks of CO_2 sequestration and increased evapotranspiration and the positive feedback of decreased albedo. These studies report that it is likely that vegetation changes will result in an overall positive feedback to Arctic warming, thus favouring near-surface permafrost degradation.

The aim of this study is twofold. First, the impact of interactive phenology on the simulated pan-Arctic land surface state for the recent past (1979-2012) is assessed by comparing an offline simulation of the Canadian Land Surface Scheme (CLASS) that has prescribed phenology, with another offline simulation of CLASS coupled to the Canadian Terrestrial Ecosystem Model (CTEM), which models phenology and other structural attributes of vegetation (leaf area index, vegetation height, canopy mass and rooting depth) interactively. The atmospheric driving data for both simulations are taken from ECMWF's ERA-Interim reanalysis (Dee *et al.*, 2011). This is followed by the assessment of the impact of interactive phenology on projected changes to the pan-Arctic land surface state, particularly near-surface permafrost, by comparing simulations with CLASS and with CLASS coupled to CTEM for the 1961-2100 period, driven by atmospheric fields from a transient climate change simulation of the 5th generation Canadian Regional Climate Model (CRCM5) for the RCP8.5 scenario.

This paper is organized as follows. Section 2.2 gives a brief description of the models used, along with a description of the simulations performed and the datasets used. Section 2.3 presents the analysis of the simulations, first by comparing them to observational datasets and then by assessing the differences introduced by interactive phenology. A brief summary and conclusions are given in section 2.4.

2.2 Methods

2.2.1 Model description

The land surface scheme CLASS (Verseghy, 1991; Verseghy *et al.*, 1993) includes prognostic equations for energy and water conservation for a user-defined number of soil layers and a thermally and hydrologically distinct snowpack where applicable (treated as an additional variable-depth soil layer). The thermal budget is

performed over all soil layers but the hydrological budget is done only for layers above bedrock. An explicit vegetation canopy has its own energy and water balance with prognostic variables for canopy temperature and water storage. In an attempt to mimic sub-grid scale variability, CLASS adopts a "pseudo-mosaic" approach and divides each grid cell into a maximum of four sub-areas: bare soil, vegetation, snow over bare soil and snow with vegetation. The energy and water budget equations are first solved for each sub-area separately and then averaged over the grid cell.

Vegetation in CLASS (Verseghy *et al.*, 1993) is represented by four plant functional types (PFTs), i.e. needleleaf trees, broadleaf trees, crops and grasses. For each PFT, certain parameters have to be prescribed, i.e. albedo, plant area index (PAI), roughness length, canopy mass and rooting depth. The canopy conductance formulation in CLASS takes into account incoming solar radiation, vapour pressure deficit, soil moisture suction and air temperature, but neglects the influence of CO_2 concentrations. With respect to phenology, the air temperature and the temperature of the top soil layer determine the timing of the transition between minimum and maximum PAI for trees. For crops, the beginning of crop growth and the end of harvest are specified as occurring on certain days of the year, depending on the latitude. Finally, grasses remain at their maximum PAI and height throughout the year, except when buried by snow. In other words, the seasonality of vegetation is modelled but not long-term variations in canopy cover or vegetation structure.

The dynamic vegetation model CTEM (Arora, 2003; Arora and Boer, 2003, 2005) includes prognostic equations for carbon mass in five pools, three being live carbon pools (leaves, stem and roots) and two dead carbon pools (litter and soil carbon). The net photosynthetic uptake, after the autotrophic respiratory losses have been taken into account, is dynamically allocated between leaves, stem, and roots. The model also estimates litter and stem fall, and root mortality, which contribute to

the litter pool. As litter decomposes it releases CO_2 and a fraction of litter becomes humidified and is transferred to the soil carbon pool.

Gross photosynthetic uptake and canopy conductance are estimated by CTEM's photosynthesis sub-module, which operates at the same time step as CLASS (30 minutes). The photosynthesis sub-module used in CTEM is based on the biochemical approach (Farquhar *et al.*, 1980). Leaf maintenance respiration is coupled to photosynthesis and is thus estimated within the photosynthesis sub-module. Autotrophic respiration from stem and root vegetation components, heterotrophic respiration from litter and soil carbon pools, allocation, and mortality losses, are modelled at a daily time step.

Processes in CTEM are modelled for nine different PFTs: evergreen and deciduous needleleaf trees, broadleaf evergreen and cold and drought deciduous trees, and C3 and C4 crops and grasses. The simulated leaf and stem biomasses are used to obtain PAI (used in energy and water balance calculations over the vegetated fraction of the grid cell), vegetation height (used to obtain the roughness length) and the heat capacity of the canopy. The root biomass is converted to a root distribution profile that is then used to estimate the fraction of roots in each soil layer required for estimating transpiration. These attributes are clustered to the four PFTs recognized by CLASS before being used in calculations.

2.2.2 Experiments

To study the effect of a deep soil configuration on the land surface state and on vegetation, two simulations are performed using CLASS coupled to CTEM, one with a 3 soil layer configuration and the other with 26 soil layers, both driven by ERA-Interim forcing data for the 1979-2012 period. These simulations will be referred to as CLASS3_CTEM/ERA and CLASS26_CTEM/ERA, respectively.

To study the effects of interactive phenology on the land surface state, another simulation (CLASS26/ERA) using CLASS with 26 soil layers and also driven by ERA-Interim forcing data for the 1979-2012 period is performed and compared to CLASS26_CTEM/ERA.

For these three simulations, the 6-hourly ERA-Interim fields (Dee *et al.*, 2011), provided at 0.75 degree resolution, are spatially assigned to the model grid cells on the basis of the nearest neighbour method. The temporal interpolation to the model timestep of 30 minutes is performed by cubic splines for the instantaneous variables (air temperature, specific humidity, wind speed and surface pressure). For longwave radiation and precipitation, fluxes are assumed to be constant during each 6 hour period. The shortwave radiation is disaggregated on the basis of the solar zenith angle, conserving energy in each 6 hour period.

To address the impact of interactive phenology on projected changes, two simulations, one with CLASS and the other with CLASS coupled to CTEM are performed and the projected changes from these two simulations compared. These simulations span the 1961-2100 period and are driven by atmospheric fields from a transient climate change simulation of CRCM5 driven by CanESM2 for the RCP8.5 scenario. These simulations will be referred to as CLASS26/CRCM and CLASS26_CTEM/CRCM, respectively.

As the 1-hourly fields from the CRCM5 simulation are provided on the same grid as the one used for this study, only temporal interpolation is required. This is achieved using the same methods as for ERA-Interim fields, except for shortwave radiation, which is now prescribed in a similar way to longwave radiation and precipitation (constant flux over 1 hour periods)./

Whenever two simulations are compared over the same period by taking the difference between them, a paired t-test is performed and only results significant at

the 5% level are reported. Similarly, when reporting projected changes, an unpaired t-test at the 5% level is employed to assess the statistical significance of these changes.

For the experiment with 3 layers, the layer thicknesses from top to bottom are 10 cm, 20 cm and 370 cm, resulting in a total soil depth of 4 m. For the experiments with 26 layers, the top four layers have thicknesses of 10 cm, 20 cm, 30 cm and 40 cm, the following ten layers have a thickness of 50 cm, the next two layers are 100 cm and 300 cm thick and the deepest ten layers have a thickness of 500 cm, for a total soil depth of 60 m. The heat flux at the bottom of the soil profile is set to zero in all cases.

To obtain initial conditions for the state of the soil and the vegetation, a two-phase spin-up is performed using CLASS coupled to CTEM. Separate spin-ups are performed for the 3 layer and 26 layer configurations, and for the ERA-Interim driven and CRCM5 driven simulations. At the beginning of the first phase, the soil temperature of all layers is set to the average air temperature of the first 10 years of the respective driving data. All moisture pools (soil water, soil ice, snow, ponded water) as well as all carbon pools (leaf, stem, root, litter, soil carbon) are initialized to zero. The CO_2 concentration is kept constant at preindustrial levels (near 278 ppm) and the first 10 years of the respective driving data are repeated until the vegetation carbon pools have reached equilibrium, which here is defined as a change of less than 1% in a 10 year period. The second phase of the spin-up starts in 1765 and runs until the start of the respective simulation, again looping over the first 10 years of the respective driving data. During this second phase, the CO_2 concentration changes each year and is prescribed from the historical CO_2 concentrations used for CMIP5 (Meinshausen *et al.*, 2011).

When CLASS is run without CTEM, the vegetation parameters discussed in section 2.2.1 have to be prescribed. These parameters are usually taken from lookup tables (Verseghy *et al.*, 1993), where their values depend on the vegetation type. For

this study, an approach similar to Garnaud *et al.* (2014b) is used. The visible and near-infrared albedos are taken from CTEM and are constant PFT dependant values. The logarithm of roughness length, the canopy mass and the rooting depth are prescribed as averages of the last 10 years of the spin-up for all PFTs except crops, and as averages of the yearly maximums of the last 10 years of the spin-up for crops. The maximum PAI is prescribed as the average of the yearly maximums of the last 10 years of the spin-up for all PFTs except grass, and as average of the last 10 years of the spin-up for grass. Finally, the minimum PAI is prescribed as the average of the yearly minimums of the last 10 years of the spin-up for tree PFTs. It is zero for crops and never used in calculations for grass.

2.2.3 Soil properties

The spatial distribution of soil types is obtained from the rasterized Digital Soil Map of the World (FAO, 1995) at 5' spatial resolution. In this dataset, each soil mapping unit is composed of up to eight soil types, of which one is dominant. For each grid cell, the fractional coverage of each soil type is determined by aggregating all mapping units inside the grid cell, including dominant and non-dominant soils.

The dataset created by Webb *et al.* (1993) is used to convert between soil types and the soil parameters required by CLASS, which are the percentages of sand and clay in each soil layer, as well as the depth to bedrock. In this dataset, each soil type is linked to a representative soil profile, which is defined as consisting of up to 14 soil horizons, and the properties given for each horizon are the percentages of sand, silt and clay, as well as the contact depths of contiguous horizons and the depth where bedrock is found. It is a common occurrence that more than one soil horizon is present in a modelled soil layer, and in these cases the sand and clay contents of the affected layer are obtained as the weighted average of the horizons, where the weights depend on the fraction of the modelled layer represented by each soil horizon.

Organic soils have distinct thermal and hydraulic properties and require a separate parameterization, as mentioned by Webb *et al.* (1993). For this study, the soil within a grid cell is considered to be completely organic when the fractional coverage of organic soils exceeds 50%. In those cases, the parameterization for deep organic soils developed by Letts *et al.* (2000) is used, where the top soil layer is assumed to consist of fibric peat, the second layer of hemic peat and any other layers above bedrock, of sapric peat. To account for organic matter within mostly mineral soils, the IGBP dataset is used (Task, 2000). As organic matter in cold climates is mostly present at and close to the surface of the soil, the approach of Paquin and Sushama (2014) is retained, which consists in replacing mineral layers by organic layers from the surface down, until the soil carbon has been distributed. A carbon content of 58% is assumed for organic matter (Pribyl, 2010).

This results in one layer (10 cm) of organic soil over most of the study domain and two layers (30 cm) over most of Scandinavia and Alaska, and also over large regions of Canada and Siberia (Figure 2.1).

2.2.4 Spatial distribution of PFTs

In CTEM, the spatial distribution of plant functional types (PFTs) can be dynamically modelled through a competition and coexistence submodule (Arora and Boer, 2006), or it can be prescribed from observational datasets. The latter approach is used in this study and the fractional areas are derived by combining two datasets for the year 2005, as discussed below.

Both datasets originate from the Moderate Resolution Imaging Spectroradiometer (MODIS). The vegetation continuous fields product (MOD44B) (Carroll *et al.*, 2011) gives the fractional coverages of trees, non-tree vegetation and bare ground at 250 m resolution. This information is aggregated within each grid cell to obtain fractional coverages of these three land cover types for each grid cell. Following a similar procedure, the land cover type product (MOD12Q1) (Friedl *et*

al., 2010) at 500 m resolution is used to obtain the fractional coverages of 12 land cover types for each grid cell. The tree fraction calculated from the MOD44B product is divided into PFTs by multiplying it by the relative abundance of the tree PFTs in the grid cell, as given by the MOD12Q1 product. Then, the non-tree vegetation fraction calculated from MOD44B is also divided into PFTs by multiplying it by the relative abundance of the non-tree PFTs in the grid cell, as given by the MOD12Q1 product.

If the fraction of non-soil types (water and ice) exceeds 99.9% of a grid cell in either product, that grid cell is considered to be irrelevant for the purposes of this study and is not simulated by the models.

Figure 2.2 shows the resulting distribution of PFTs over the study domain, with needleleaf trees dominating central Canada, the southern half of Siberia and northeastern Europe. Broadleaf trees occur to the south of this boreal forest, being especially abundant over the eastern US. Crops cover large areas of Europe, the northern US and southern Canada, as well as southern Russia and northern China. Grasses (which include all short natural vegetation) are by far the most abundant PFT, dominating large areas north of the tree line. Finally, bare ground is the dominant type only in the high Arctic and the Gobi desert for the pan-Arctic domain considered in this study.

2.2.5 Validation data

Estimation of vegetation attributes over large regions and relatively long periods can currently only be achieved by remote sensing. Most remote sensing algorithms make use of the absorption of photosynthetically active radiation (PAR) by vegetation, which results in lower reflectivities in the PAR spectrum over densely vegetated regions when compared to regions with less vegetation. The retrieval of reflectivities is often hindered by cloud cover and high solar zenith angles over high latitude regions. Additionally, the conversion of reflectivities into vegetation

attributes, such as leaf area index or primary productivity, is not straightforward and numerous assumptions have to be made. Nonetheless, remote sensing estimates agree relatively well with field observations and are the only available data when model performance is to be assessed over large regions.

To validate the simulated plant area index (PAI), the dataset from the International Satellite Land Surface Climatology Project, Initiative II (ISLSCP II) is used (Sietse, 2010). This dataset gives monthly estimates of PAI at 0.25 degree resolution for the period from 1982 to 1998. The data within each grid cell is aggregated and the comparison is done on the model grid.

To validate the simulated gross and net primary productivities (GPP and NPP), the MOD17A3 dataset derived from MODIS is used (Zhao *et al.*, 2005). This dataset gives yearly estimates of GPP and NPP at 1 km resolution, and is available from the year 2000 until the current period. The data within each grid cell is aggregated and the comparison is done on the model grid.

The soil carbon pool simulated by CTEM can be validated against the estimates of IGBP (Task, 2000) at 5' spatial resolution, which are based on the Digital Soil Map of the World (FAO, 1995). Over permafrost regions, the Northern Circumpolar Soil Carbon Database (NCSCD) provides a more recent estimate at 0.012 degree resolution (Hugelius *et al.*, 2013). In all cases, only the soil carbon in the first meter of soil is taken into account when performing the validation.

Estimates of permafrost extent are generally obtained from field surveys. For this study the map from Brown *et al.* (1997) is used to validate the modelled permafrost extent. In this map, permafrost is categorized according to its areal extent into continuous (>90% coverage), discontinuous (50% to 90% coverage), sporadic (10% to 50% coverage) and isolated (<10% coverage). For this study, a grid cell is

said to have near-surface permafrost when the modelled temperature of at least one soil layer in the top 5 m remains at or below 0 °C for 24 consecutive months.

Another validation can be done by comparing simulated and observed values of active layer thickness (ALT), where ALT is defined as the maximum annual thaw depth. The circumpolar active layer monitoring (CALM) dataset from Brown *et al.* (2000) contains yearly observations of ALT at specific sites, starting in 1990. ALT is estimated using a variety of methods, including mechanical probing with steel rods, thaw tubes and interpolation from ground temperature measurements at different depths. In the model, the ALT for a particular year is assumed to be the average depth of the soil layer closest to the surface with temperatures at or below 0 °C during the year under consideration.

2.3 Results

2.3.1 Validation

When comparing the 1982-1998 averages of plant area index (PAI) simulated by CLASS26_CTEM/ERA to remote sensing estimates over the study domain (Figure 2.3), it is evident that there is high level of agreement in the overall spatial pattern. Some overestimation by CLASS26_CTEM/ERA can be seen in the boreal forests of eastern Canada and western Russia. Significant underestimation is found over the broadleaf forest regions of the eastern US, probably linked to cooler spring and summer soil temperatures, brought by the addition of a layer of organic matter at the surface. Underestimation can also be found in the needleleaf deciduous forest regions of Siberia and some underestimation is also evident for the northern parts of Alaska, Canada and Siberia.

The CLASS26_CTEM/ERA simulation captures the spatial distribution of the 2000-2010 average net primary productivity (NPP) when compared with remote sensing estimates (Figure 2.4). However, significant overestimation of NPP can be

seen over the boreal forests of Canada and Russia, while underestimation is mostly confined to regions where croplands are predominant, like the Northern Plains and western Europe. Gross primary productivity (GPP) is highly correlated to NPP and exhibits the same spatial patterns and biases as NPP (not shown).

Figure 2.5 compares the soil carbon density simulated by CTEM in the CLASS26_CTEM/ERA simulation to those from IGBP and NCSCD. It is important to note that the transient soil carbon pool simulated by CTEM does not interact with CLASS, meaning that the prescribed number of organic layers (Figure 2.1) remains unchanged through the simulation. Work is in progress to couple CTEM's soil carbon pool to CLASS (Joe Melton, personal communication). The comparison shows that CLASS26_CTEM/ERA generally has higher soil carbon than the IGBP estimate, except for peatlands in central Russia and central Canada. Comparison of CLASS26_CTEM/ERA with the recent NCSCD estimate suggests good agreement over Siberia. However, significant biases are observed over North America.

Garnaud *et al.* (2014a) studied the effects of driving data on simulated vegetation over North America, using a previous version of CTEM coupled to CLASS. They reported good performance in simulating PAI, GPP and NPP, except for western Canada, where CTEM showed considerable underestimation. The present study presents much better performance over western Canada, which is partly due to adjustments done to the parameters of needleleaf evergreen trees, which are now more resistant to drought and cold conditions and have a higher photosynthetic rate. These adjustments might also be responsible for the overestimation of PAI and NPP over the needleleaf evergreen forest regions of eastern Canada and Russia.

CLASS26_CTEM/ERA realistically captures the spatial extent of near-surface permafrost, as can be seen in Figure 2.6. The CLASS26/ERA simulation performs equally well, and almost all regions where observations show more than 50%

permafrost coverage are properly captured by both simulations, including small patches over northern Mongolia.

When comparing simulated and observed active layer thickness (ALT), it is important to consider that observations are only representative of a very small area within a much larger grid cell. In Figure 2.7, the simulated ALTs from CLASS26_CTEM/ERA and CLASS26/ERA are compared to observations at the CALM network sites. Factors such as complex terrain, heterogeneity of soil properties within the grid cell, biases in the driving data and model error are mostly responsible for the spread around the 1:1 line. Nonetheless, these results show a considerable improvement over a previous study by Paquin and Sushama (2014), where CLASS showed almost exclusively overestimation of the ALT. This improvement can be attributed to changes in the prescribed depth to bedrock and changes to the prescribed number of layers of organic matter, both of which act to increase the total soil moisture content, resulting in an increased thermal inertia, which causes a good part of the energy available during summer to be used for thawing the frozen water in the soil instead of penetrating deeper into the soil column.

2.3.2 Impact of deep soil column

While the top two layers of CLASS3_CTEM/ERA and CLASS26_CTEM/ERA are identical, the thick third layer of CLASS3_CTEM/ERA is replaced by 8 thin layers in CLASS26_CTEM/ERA and 16 more layers are added at the bottom. Differences between the simulations are caused by the increased vertical resolution below 0.3 m, which affects the movement of soil water and the freeze-thaw dynamics. Additional differences arise because of the displacement of the zero heat flux boundary from 4 m below the surface in CLASS3_CTEM/ERA to 60 m below the surface in CLASS26_CTEM/ERA, and also because of a working

assumption of zero heat flux at the bottom of the third soil layer made when initially solving the surface energy balance.

Statistically significant differences between CLASS26_CTEM/ERA and CLASS3_CTEM/ERA in the maximum temperature of the first soil layer are shown in Figure 2.8a. Cooler maximum temperatures are observed in CLASS26_CTEM/ERA over a large part of the domain, extending slightly beyond the southern limit of the permafrost regions, but not for the most northern regions of the domain. Minimum temperatures of the first soil layer (Figure 2.8b) show the opposite signal, implying that the main difference between CLASS3_CTEM/ERA and CLASS26_CTEM/ERA is in the amplitude of the yearly cycle.

The regions where the 26 layer configuration induces significant dampening of the yearly cycle are those where the thick third layer (in CLASS3_CTEM/ERA) contains ice for at least part of the year. In permafrost regions, CLASS3_CTEM/ERA maintains a higher vertically integrated ice content, regardless of having warmer temperatures in the first two soil layers. The explanation for this is that in CLASS3_CTEM/ERA the heat flux between the second and third soil layer is much smaller than in CLASS26_CTEM/ERA, due to the assumption of zero heat flux at the bottom of the third soil layer made when solving the energy balance at the surface. This assumption, coupled with an assumed quadratic temperature profile in the top three soil layers, results in an abnormally large temperature gradient (leading to a high heat flux) at the interface between the second and third soil layers in the CLASS26_CTEM/ERA simulation.

The impact of a deep soil column on the annual maximum PAI (Figure 2.9a) is generally modest, with the differences between both simulations being generally below 0.5 m^2 m^{-2}. A clear spatial pattern emerges, with higher PAI concentrated over permafrost regions and lower PAI mostly over forested permafrost-free regions in CLASS26_CTEM/ERA compared to CLASS3_CTEM/ERA. These differences in

PAI are very strongly correlated to the differences in moisture availability in the rooting zone (Figure 2.9b), with higher (lower) water availability resulting in higher (lower) PAI, showing the capability of CTEM to simulate the response of vegetation to water availability.

2.3.3 Impact of interactive phenology (recent past)

To study the impact of interactive phenology, CLASS26/ERA and CLASS26_CTEM/ERA are compared. In the CLASS26/ERA simulation only the seasonality of vegetation is represented, as the annual maximum and minimum PAI are prescribed along with all other vegetation related parameters. In the CLASS26_CTEM/ERA simulation, vegetation can adapt to climate and PAI as well as all other vegetation parameters are dynamic functions of climate, soil conditions and CO_2 concentrations.

Figure 2.10a shows that CLASS26_CTEM/ERA simulates higher maximum PAI over most of the study domain, with the exception of some parts of Europe and the region to the south of the Great Lakes. The higher PAI values are easily explained by increased photosynthesis due to the CO_2 fertilization effect and warming temperatures in the past few decades. The regions where PAI is similar in both simulations are regions where temperature plays a lesser role in controlling photosynthesis, resulting in water availability being the main control on vegetation.

It is important to note that although the maximum PAI is higher in CLASS26_CTEM/ERA over most of the domain, the PAI values during the year might not follow the same pattern. This is exemplified in Figure 2.10b, which shows the average PAI during the month of June. It can be seen that CLASS26_CTEM/ERA has mostly lower PAI values during this month than CLASS26/ERA, with the exception of some regions dominated by needleleaf evergreen forests. The explanation for this is that in CLASS26/ERA vegetation reaches its maximum PAI during early summer, while the maximum values of PAI don't occur until late

summer in the CLASS26_CTEM/ERA simulation. This has been recognized as a problem and will be corrected in future versions of CTEM (Joe Melton, personal communication).

PAI is one of the variables strongly related to evapotranspiration (ET), and higher ET is expected when PAI is higher. Figure 2.11a shows that ET is only higher for the regions with the largest differences in maximum PAI, while a lower ET occurs in many regions, including some in which maximum PAI is higher. This apparent contradiction can be explained by taking into account that the highest values of ET occur during early summer, coinciding with the time of the year where PAI is lower in the CLASS26_CTEM/ERA simulation. Another factor might be that the parameterization of stomatal resistance also changes between the two simulations, and increasing CO_2 concentrations will result in CTEM simulating higher stomatal resistances, leading to lower ET.

The differences in ET between both simulations have important repercussions on other components of the water cycle, as shown in Figure 2.11b, where the regions showing higher (lower) ET also show lower (higher) runoff, thus conserving the water mass balance. Total integrated soil moisture content (not shown) presents differences of the same sign as runoff.

The repercussions of differences in ET also affect the energy balance at the surface through evaporative cooling, where higher (lower) ET will cause lower (higher) summer temperature of the first soil layer as can be seen in Figure 2.12a. A cooler soil during the summer results in shallower active layer thickness at the southern limit of the permafrost region, as is shown in Figure 2.12b.

The differences in albedo caused by higher PAI are very small, in part due to the prescribed albedo of organic soils (0.175), which is equal to the albedo of grass and only slightly larger than the albedo of needleleaf trees (0.11). Another factor

influencing the albedo is the parameterization of snow albedo, which is allowed to be refreshed by snow unloading from vegetation. This unloading occurs more often in the CLASS26_CTEM/ERA simulation, as higher winter PAI results in the interception of more snow by the canopy.

2.3.4 Impact of interactive phenology on projected changes

In order to study the simulated impact of interactive phenology on the land surface state during the 21st century, a simulation with CLASS (CLASS26/CRCM) and a simulation with CLASS coupled to CTEM (CLASS26_CTEM/CRCM) are compared. The driving variables for these simulations are taken from a CRCM5 simulation. It has been shown by Garnaud *et al.* (2014a) that driving data (especially precipitation) can have an important impact on the vegetation simulated by CTEM. Nevertheless, vegetation attributes such as PAI, GPP and NPP continue to have values very similar to those of CLASS26_CTEM/ERA and observational estimates during the 1981-2010 period, and permafrost extent and ALT continue to be well represented, with agreements (with respect to observations) similar to CLASS26_CTEM/ERA during the 20th century.

Figure 2.13 summarizes projected changes to the important atmospheric fields used to drive CLASS26/CRCM and CLASS26_CTEM/CRCM. Increases of 4 to 10 K in mean air temperature are projected for most of the domain, with the greatest increases in the northernmost regions. As the warmer air can hold more humidity, the specific humidity also increases over the whole domain. Significant increases in annual precipitation are expected for the colder regions, as a result of increases of precipitation in all seasons except during summer (JJA). Decreases in summer precipitation are especially pronounced over Europe (not shown). Significant changes in the incoming shortwave radiation due to changes in cloudiness are also projected, with decreases over large portions of the domain and increases limited to western Europe.

Projected changes to the spring PAI are shown in Figure 2.14a for CLASS26_CTEM/CRCM and in Figure 2.14b for CLASS26/CRCM. In CLASS26/CRCM, PAI increases due to early snow melt and therefore an earlier start of the growing season. In CLASS26_CTEM/CRCM vegetation additionally benefits from the CO_2 fertilization effect, which is evidenced by generally larger increases in PAI, but it can also be affected by drought stress, which plays a role mainly over Europe.

Spring evapotranspiration shows important increases in both CLASS26_CTEM/CRCM and CLASS26/CRCM over most of the domain (Figures 2.14c and 2.14d). These increases result from the increased atmospheric demand for water and benefit from the increased PAI. It is interesting to note that CLASS26_CTEM/CRCM projects smaller increases in ET than CLASS26/CRCM, despite having generally larger PAI. This is due to the increased stomatal resistance simulated by CTEM in response to high CO_2 concentrations in future climate, which reduces ET per unit PAI in CLASS26_CTEM/CRCM.

Both CLASS26_CTEM/CRCM and CLASS26/CRCM project important near-surface permafrost degradation, as can be seen in Figures 2.14e and 2.14f. More than half of the grid cells with near-surface permafrost in the 1981-2010 period become permafrost free by 2071-2100, and the remaining grid cells present important increases in ALT. This is consistent with the projections of CMIP5 models presented in Slater and Lawrence (2013) and Koven *et al.* (2013).

Figure 2.15 shows the progression of the differences in ALT between CLASS26_CTEM/CRCM and CLASS26/CRCM for each 30-year period between 1981 and 2100. For the 1981-2040 period (Figure 2.15a and 2.15b), the most important differences are concentrated at the southern limit of the permafrost region, with CLASS26_CTEM/CRCM having shallower ALT due to higher evaporative cooling, with a similar pattern to Figure 2.12b, discussed in section 2.3.3. For the

2041-2070 period (Figure 2.15c) and especially for the 2071-2100 period (Figure 2.15d), the ALT remains shallower in CLASS26_CTEM/CRCM near the southern limit of the future near-surface permafrost, but is deeper for the rest of the future permafrost region, pointing towards a positive feedback of vegetation on permafrost degradation. This feedback arises from a combination of less snow leading to lower albedos and higher stomatal resistances leading to lower ET in CLASS26_CTEM/CRCM.

2.4 Summary and conclusions

The impact of interactive phenology on the simulated pan-Arctic land surface is assessed by comparing two simulations of CLASS - one with interactive phenology (i.e. CTEM) and the other with prescribed phenology. These simulations are first performed for the 1979-2012 period, using atmospheric forcing from the ERA-Interim reanalysis, and then for the 21st century, using atmospheric forcing derived from an existing transient climate change simulation of CRCM5 for RCP8.5.

The ability of CTEM to simulate the most important variables of the pan-Arctic terrestrial biosphere was assessed by comparing to observational estimates. This comparison suggests that the model is able to correctly reproduce the general spatial pattern of PAI and NPP, improving on certain important biases found by previous studies and providing results with a quality comparable to other state-of-the-art models (Murray-Tortarolo *et al.*, 2013). The soil carbon pool simulated by CTEM is significantly larger than the IGBP estimates. It is in better agreement with the recent NCSCD estimates over Siberia, but not over North America.

Permafrost extent was remarkably well simulated when using the deep soil configuration and the depth of the active layer was also captured reasonably well when comparing to observations and other modelling studies (Koven *et al.*, 2013;

Slater and Lawrence, 2013). The large biases observed in a previous study with CLASS were improved significantly by indirectly increasing the thermal inertia of the soil.

In accordance with previous modelling studies, the vegetation in CTEM responds to warming temperatures and increasing CO_2 concentrations by increased photosynthetic activity and growth. The ability of vegetation in CTEM to respond to increasing CO_2 concentrations also results in slightly slower increases in transpiration during the 21st century, when compared to CLASS.

The assessment of the impacts of adding CTEM are complicated by the differences in the seasonal cycle of vegetation, with vegetation in CTEM peaking (incorrectly) several months later than in CLASS and observations. This late peak is also present in several other vegetation models, as discussed in Murray-Tortarolo *et al.* (2013). Nevertheless, the differences between both simulations in terms of evapotranspiration, runoff, soil temperature and active layer thickness behave in a physically congruent manner, which provides confidence in the ability of CLASS coupled to CTEM to simulate the current and future states of the land surface, including terrestrial ecosystems.

Under a high emission scenario, such as the one used for this study, significant near-surface permafrost degradation is projected, with the degradation being accelerated by the inclusion of CTEM during the second half of the 21st century, as a result of the albedo feedback and reduced evapotranspiration.

As large changes in evapotranspiration were observed by adding CTEM, it becomes necessary to explore the effect of these changes on the pan-Arctic climate, as feedbacks on cloud cover and precipitation are expected. This will be achieved by doing simulations with a regional climate model, CRCM5, which uses CLASS to simulate the land surface and CTEM for the terrestrial biosphere. Future studies will

also explore the ability of CTEM to simulate disturbance and competition between PFTs, as well as the effect of these processes on the land surface and on climate.

FIGURES

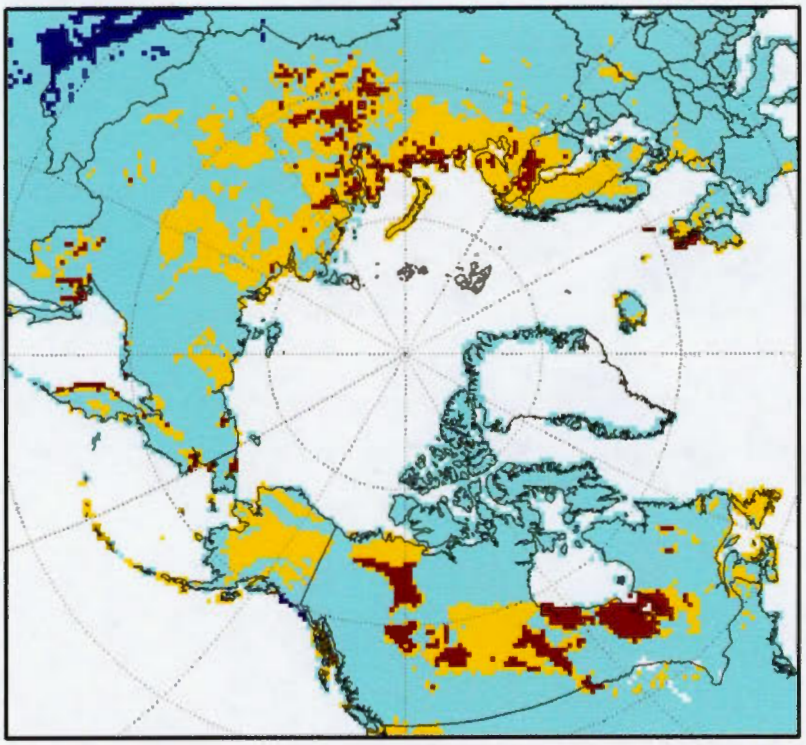

Figure 2.1 Number of prescribed organic soil layers : dark blue is used for grid cells with 0 layers, cyan for 1 layer (10 cm), yellow for 2 layers (30 cm) and red for deep organic soils.

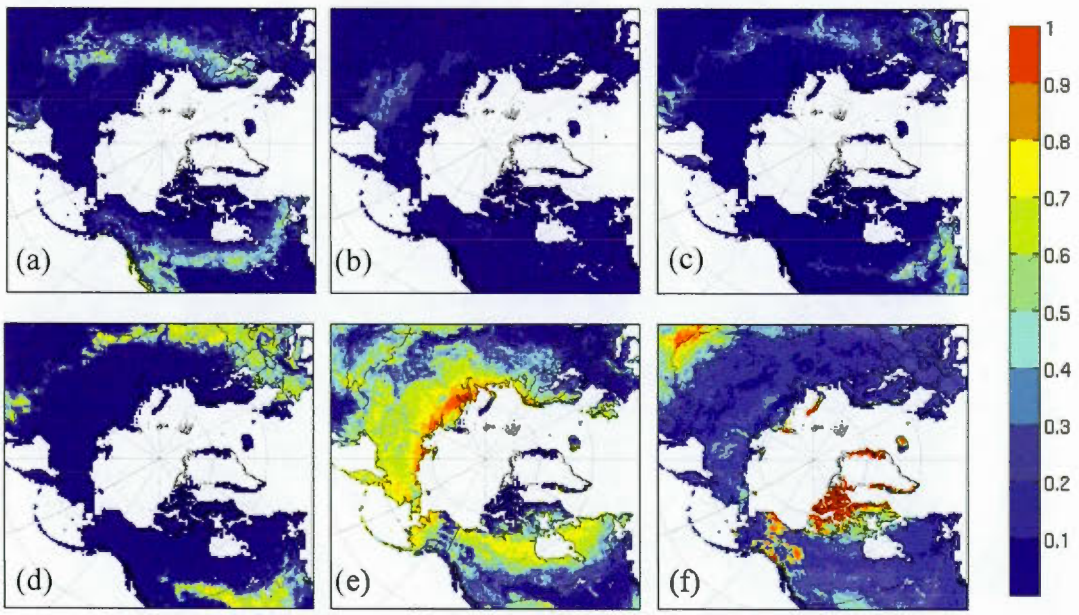

Figure 2.2 Prescribed fractional coverages of plant functional types : (a) needleleaf evergreen trees, (b) needleleaf deciduous trees, (c) broadleaf deciduous trees, (d) crops, (e) grasses, (f) bare soil.

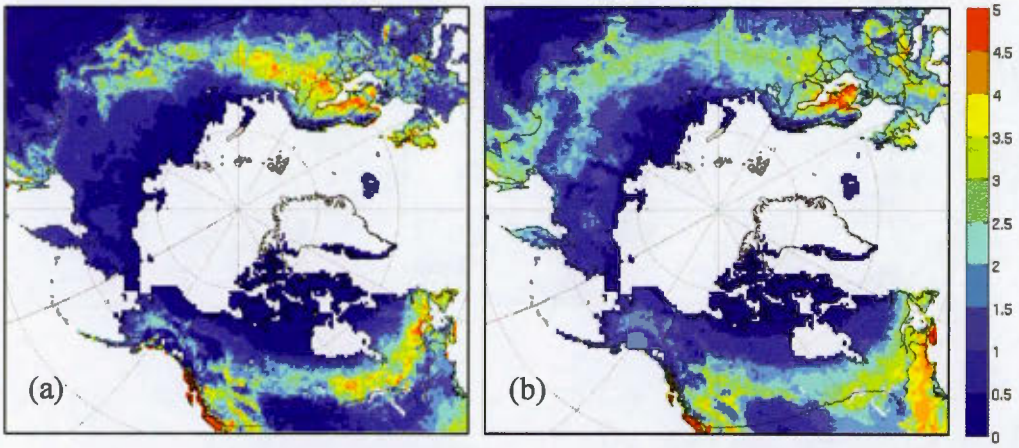

Figure 2.3 Mean PAI [m^2 m^{-2}] for the 1982-1998 period from (a) CLASS26_CTEM/ERA, (b) ISLSCP II.

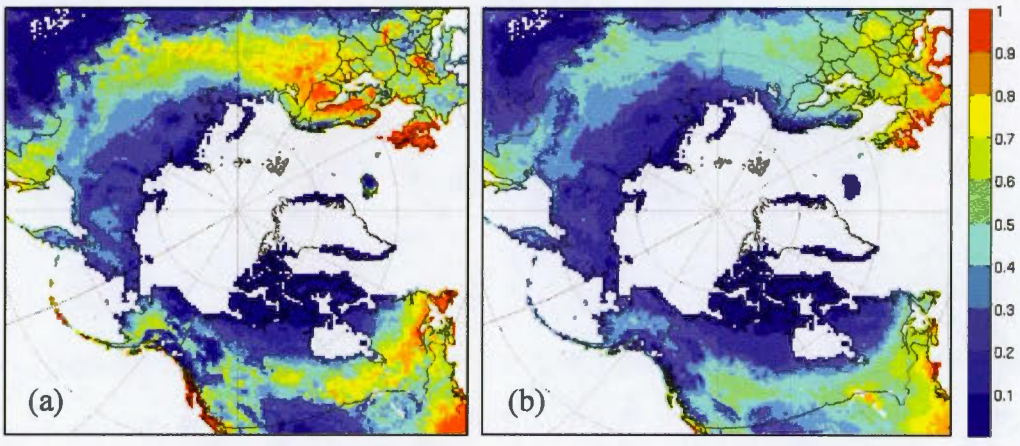

Figure 2.4 Mean NPP [kgC m^{-2} yr^{-1}] for the 2000-2010 period from (a) CLASS26_CTEM/ERA, (b) MODIS.

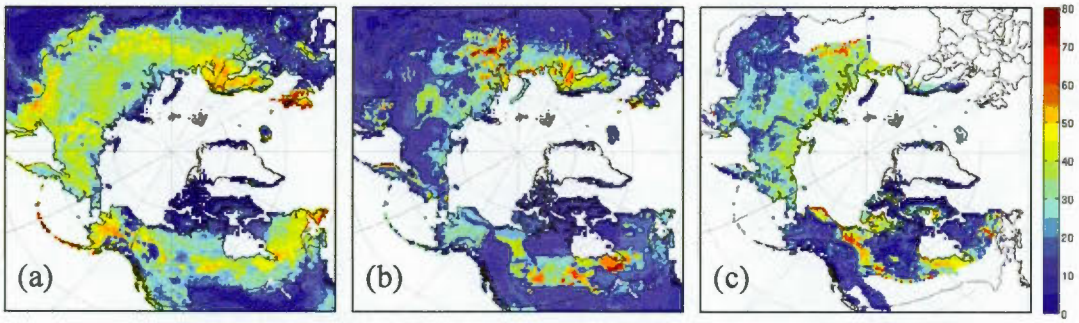

Figure 2.5 Soil carbon density [kg m^{-2}] from (a) CLASS26_CTEM/ERA for the 1981-1990 period, (b) IGBP, (c) NCSCD.

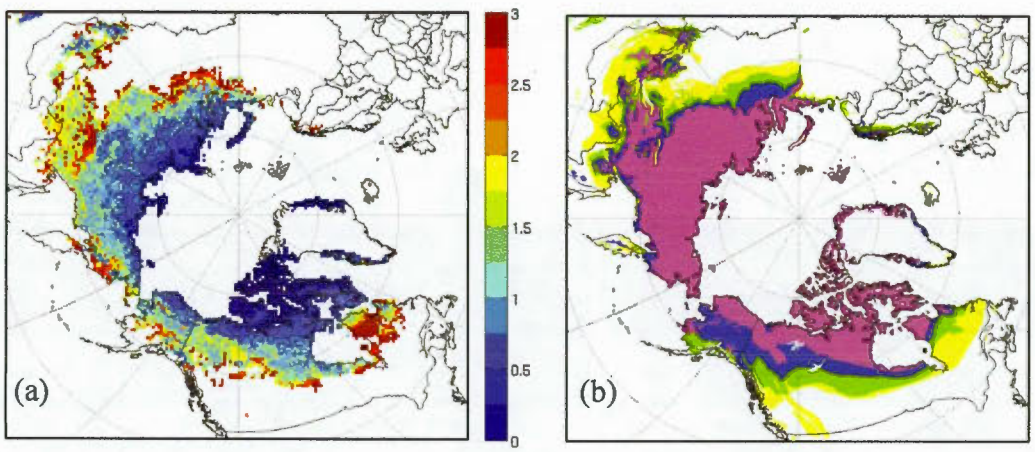

Figure 2.6 (a) Mean 1981-1990 active layer thickness [m] of near-surface permafrost, simulated by CLASS26_CTEM/ERA. (b) Observed permafrost extent: magenta, continuous (>90%); blue, discontinuous (50-90%); green, sporadic (10-50%); yellow, isolated (<10%).

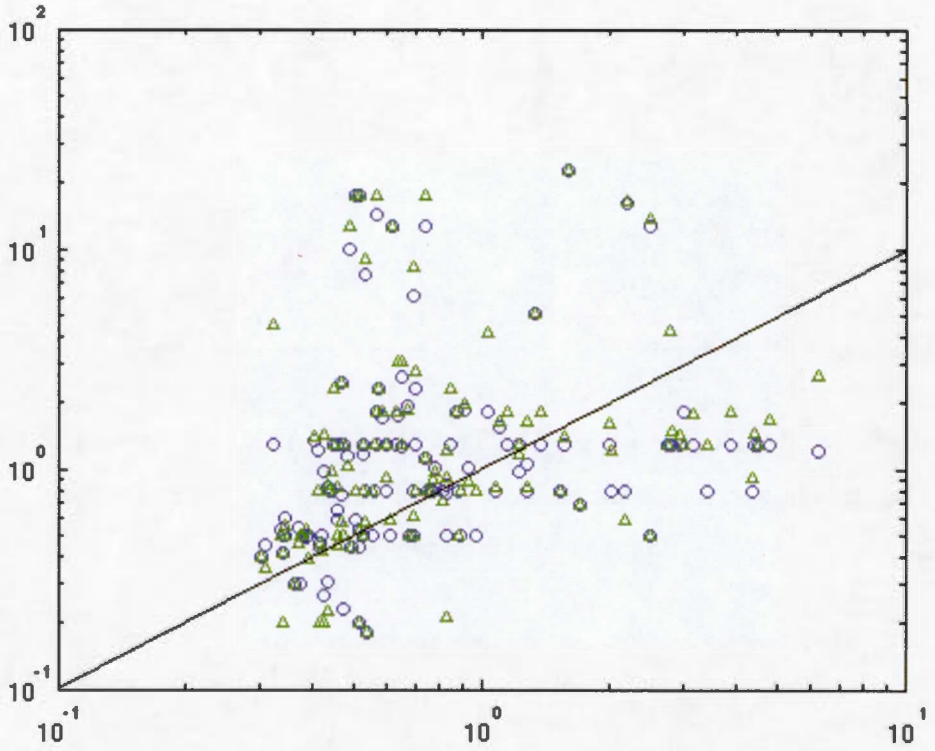

Figure 2.7 Comparison between modelled and observed ALT [m] for the 1990-2012 period. Here blue circles are used for CLASS26_CTEM/ERA and green triangles for CLASS26/ERA.

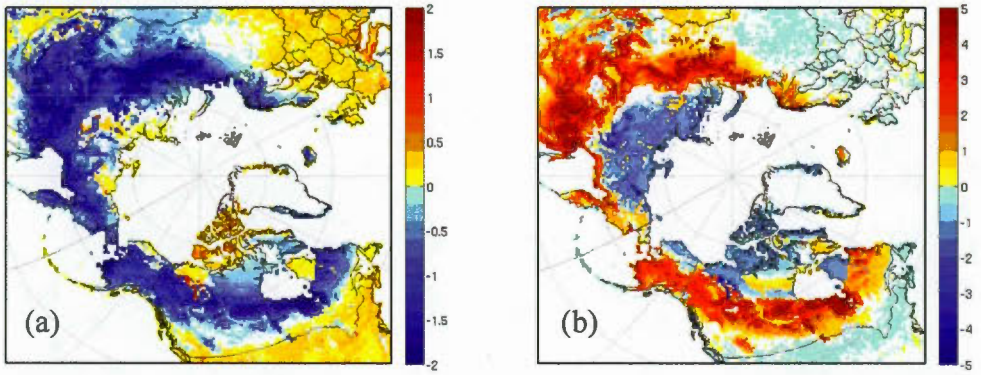

Figure 2.8 (a) Difference (CLASS26_CTEM/ERA - CLASS3_CTEM/ERA) in 1981-2010 annual maximum temperature [K] of the first soil layer. (b) Same, but for annual minimum temperature.

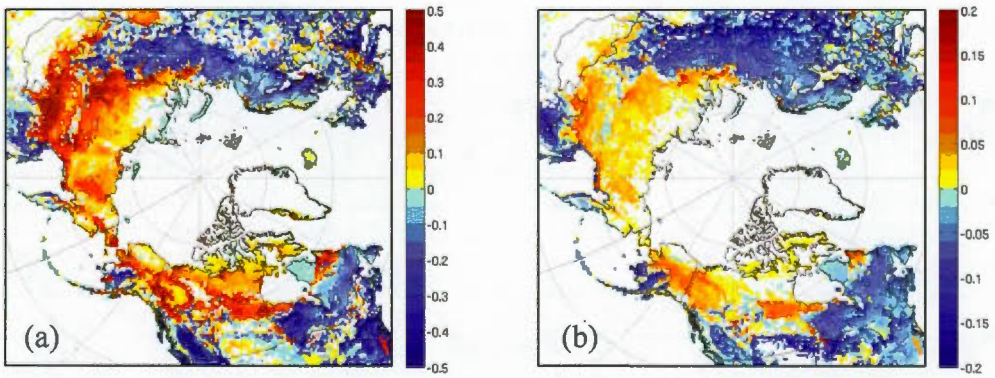

Figure 2.9 (a) Difference (CLASS26_CTEM/ERA - CLASS3_CTEM/ERA) in 1981-2010 annual maximum PAI [m^2 m^{-2}]. (b) Same, but for average root zone moisture availability (adimensional : equal to zero at the wilting point and below, equal to one at field capacity and above).

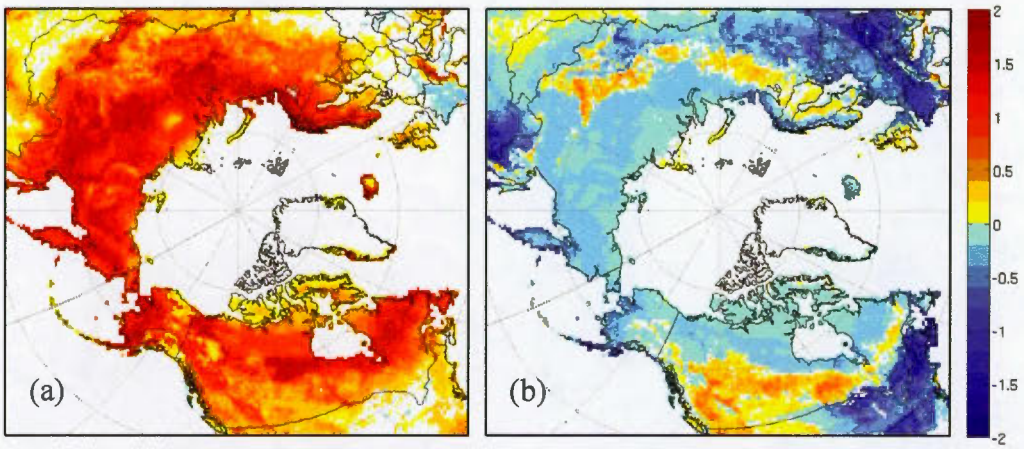

Figure 2.10 (a) Difference (CLASS26_CTEM/ERA - CLASS26/ERA) in 1981-2010 annual maximum PAI [m^2 m^{-2}]. (b) Same, but for PAI during June.

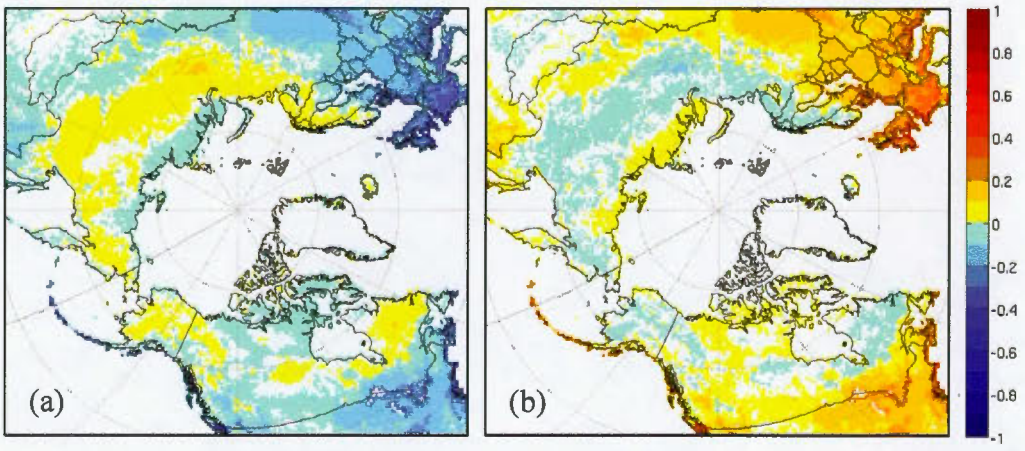

Figure 2.11 (a) Difference (CLASS26_CTEM/ERA - CLASS26/ERA) in 1981-2010 average evapotranspiration [mm day^{-1}]. (b) Same, but for average runoff.

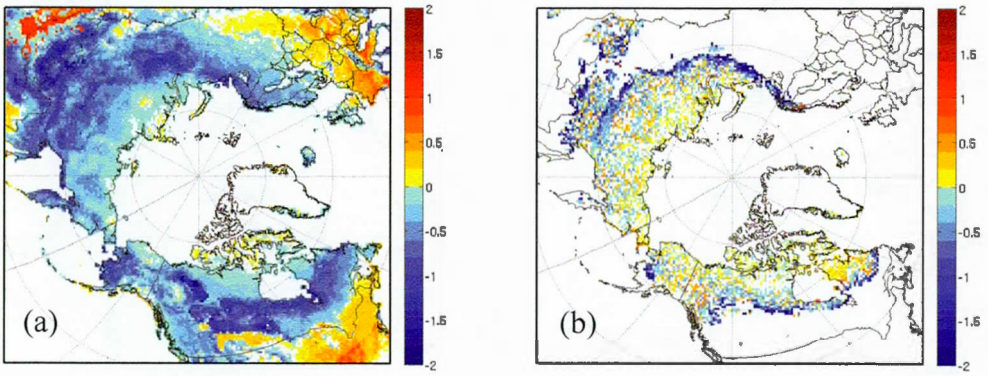

Figure 2.12 (a) Difference (CLASS26_CTEM/ERA - CLASS26/ERA) in 1981-2010 summer temperature [K] of the first soil layer. (b) Same, but for ALT [m].

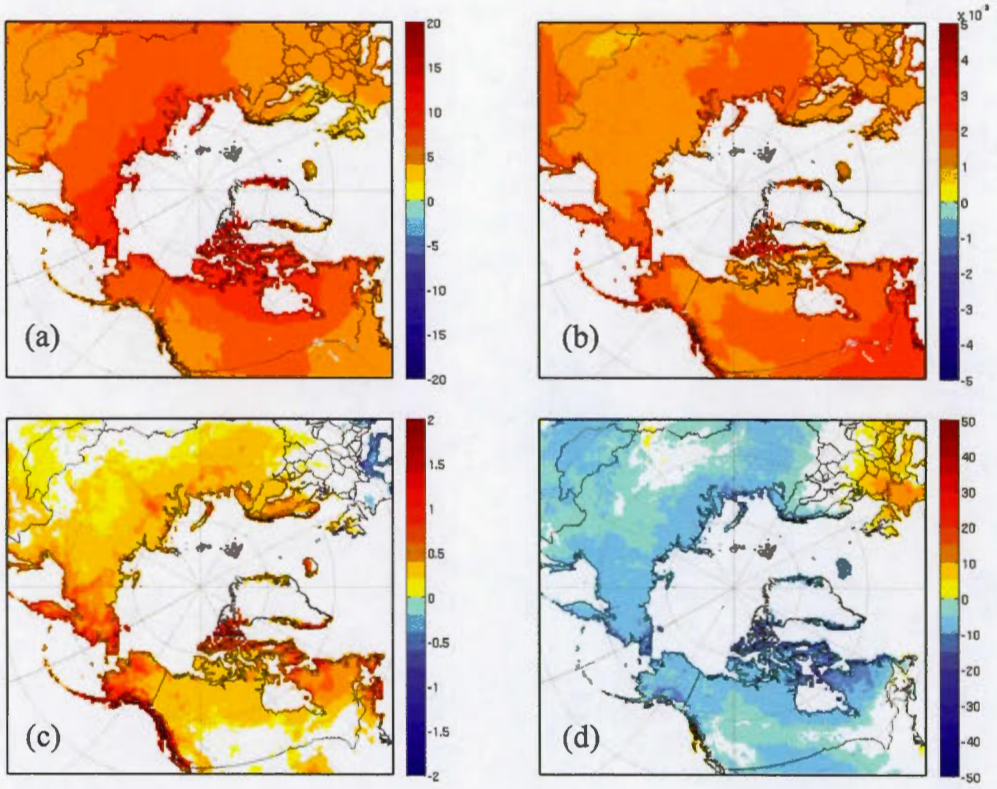

Figure 2.13 Projected changes (2071-2100 average minus 1981-2010 average) in driving data : (a) air temperature [K], (b) air specific humidity [kg kg^{-1}], (c) precipitation [mm day^{-1}], (d) incoming shortwave radiation [W m^{-2}].

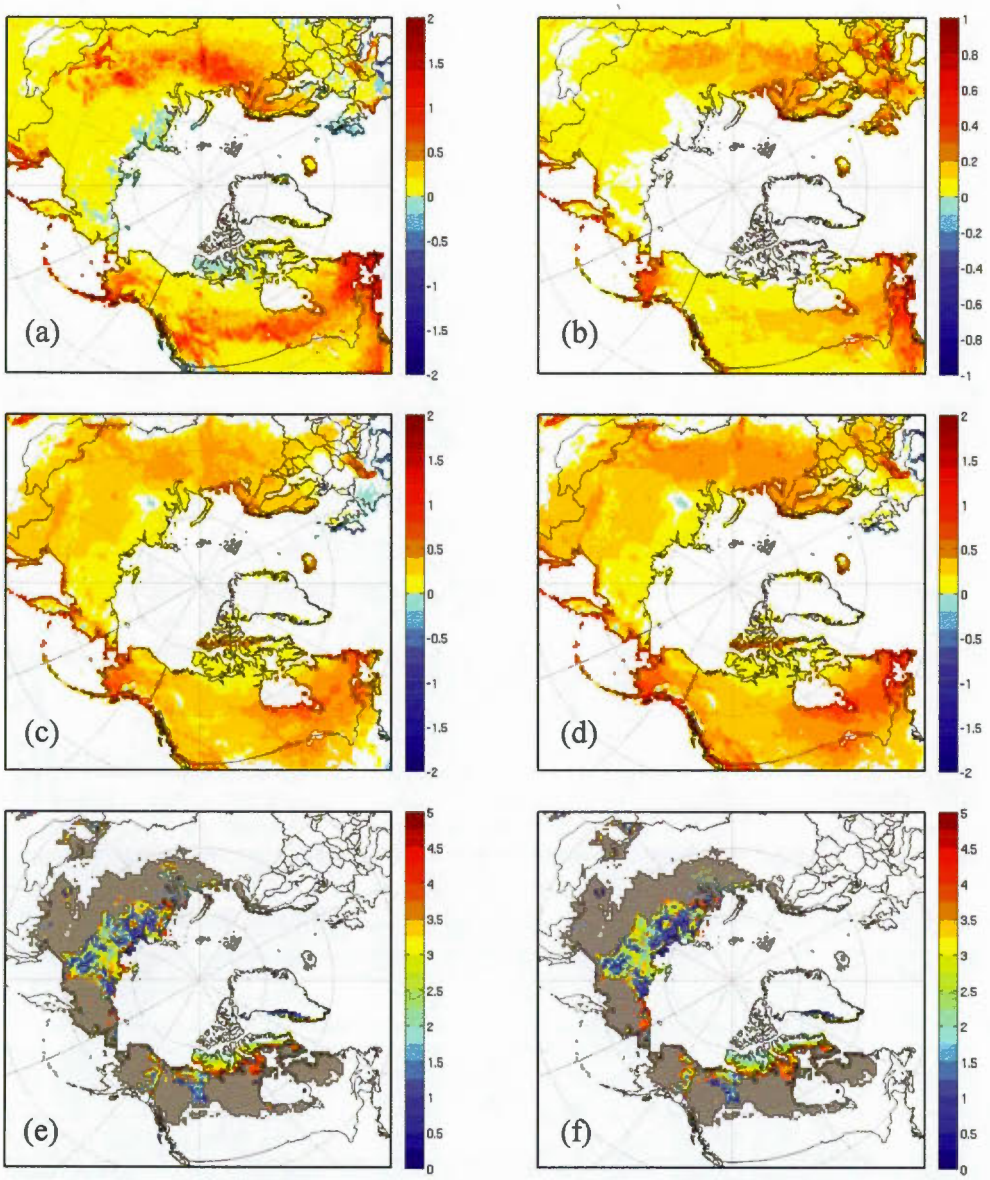

Figure 2.14 Projected changes (2071-2100 minus 1981-2010) in : (a,b) spring PAI [m^2 m^{-2}], (c,d) spring ET [mm day^{-1}], (e,f) ALT [m], from CLASS26_CTEM/CRCM in the first column (a,c,e), and from CLASS26/CRCM in the second column (b,d,f). Grey areas in (e,f) represent regions where permafrost in the top 5 meters of soil degraded completely by 2071-2100.

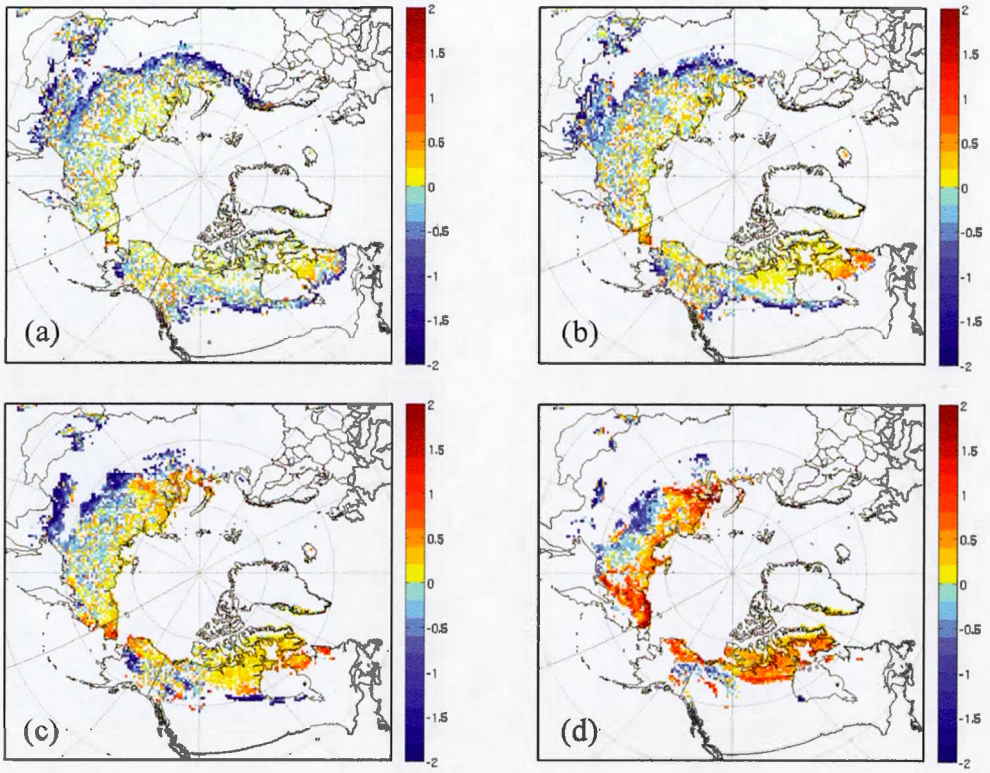

Figure 2.15 Differences (CLASS26_CTEM/CRCM - CLASS26/CRCM) in ALT [m] for the (a) 1981-2010 period, (b) 2011-2040, (c) 2041-2070, (d) 2071-2100.

CHAPTER III

CONCLUSION

This study focuses mainly on the impacts of adding a dynamic vegetation model, CTEM, to offline runs of a land surface scheme, CLASS, over the pan-Arctic domain. Special attention was given to the representation of the soil, including organic soils and depth to bedrock, in order to simulate an appropriate thermal inertia, necessary for a good representation of permafrost.

The ability of CLASS+CTEM to simulate the most important structural descriptor of vegetation, the plant area index, was assessed by comparing to satellite estimates. The model reproduces the general spatial pattern of PAI reasonably well, improves on certain important biases found by previous studies and provides results with a quality comparable to other state-of-the-art models (Murray-Tortarolo *et al.*, 2013).

The simulated land-atmosphere fluxes of carbon were also validated against an independent set of satellite estimates, by comparing the modelled primary productivities (GPP and NPP) of vegetation to their observational counterparts. Again, the model was able to capture the overall spatial pattern, giving results comparable in quality to other models.

The soil carbon pool simulated by CTEM is significantly larger than the IGBP estimates. It is in better agreement with the recent NCSCD estimates over Siberia, but not over North America.

Permafrost extent was remarkably well simulated when using the deep soil configuration and the depth of the active layer was also captured reasonably well when comparing to observations and other modelling studies (Koven *et al.*, 2013; Slater and Lawrence, 2013). The large biases observed in ALT during a previous study with CLASS were improved significantly due to the increased thermal inertia.

The impact of using a deeper and more discretized soil column on the thermal and hydraulic behaviour of the soil was assessed, and it was found that important differences exist, especially over regions undergoing the annual freeze-thaw cycle, including regions underlain by permafrost. These differences are caused by complex interactions between the effects of increased vertical discretization, added soil layers and the parameterization used to solve the surface energy balance.

Another important finding from studying the effects of the deep soil configuration was that vegetation in CTEM is moderately sensitive to water stress over the study domain, as very high correlations were found between differences in available soil moisture and PAI.

In accordance with previous modelling studies, vegetation in CTEM responds to warming temperatures and increasing CO_2 concentrations by increased photosynthetic activity and growth. The ability of vegetation in CTEM to respond to increasing CO_2 concentrations also results in slightly slower increases in transpiration during the 21st century, when compared to CLASS.

The assessment of the impacts of adding CTEM are complicated by the differences in the seasonal cycle of vegetation, with vegetation in CTEM peaking (incorrectly) several months later than in CLASS and observations, but future versions of CTEM will correct this problem. This late peak is also present in several other vegetation models, as discussed in Murray-Tortarolo *et al.* (2013).

Nevertheless, the differences between both simulations in terms of evapotranspiration, runoff, soil temperature and active layer thickness behave in a physically congruent manner, which provides confidence in the ability of these models to simulate the current and future states of the land surface, including terrestrial ecosystems.

Under a high emission scenario, such as the one used for this study, significant near-surface permafrost degradation is projected, with the degradation being accelerated by the inclusion of CTEM during the second half of the 21st century, as a result of the albedo feedback and reduced evapotranspiration.

As large changes in evapotranspiration were observed by adding CTEM, it becomes necessary to explore the effect of these changes on the pan-Arctic climate, as feedbacks on cloud cover and precipitation are expected. This can be achieved by doing simulations with a regional climate model, CRCM5, which uses CLASS to simulate the land surface and can be coupled to CTEM.

In this study the full potential of CTEM was not exploited, as only the basic modules of CTEM were enabled, a recommended step when a model is used for the first time over a certain region. Future studies will explore the ability of CTEM to simulate disturbance and competition between PFTs, as well as the effect of these processes on the land surface and on climate.

Finally, the soil carbon pool simulated by CTEM does not currently influence the thermal and hydraulic properties of the soil simulated by CLASS. A parameterization coupling these properties to CTEM would improve the physical consistency of the model, giving higher confidence in its projections.

APPENDIX A

SUPPLEMENTARY FIGURES

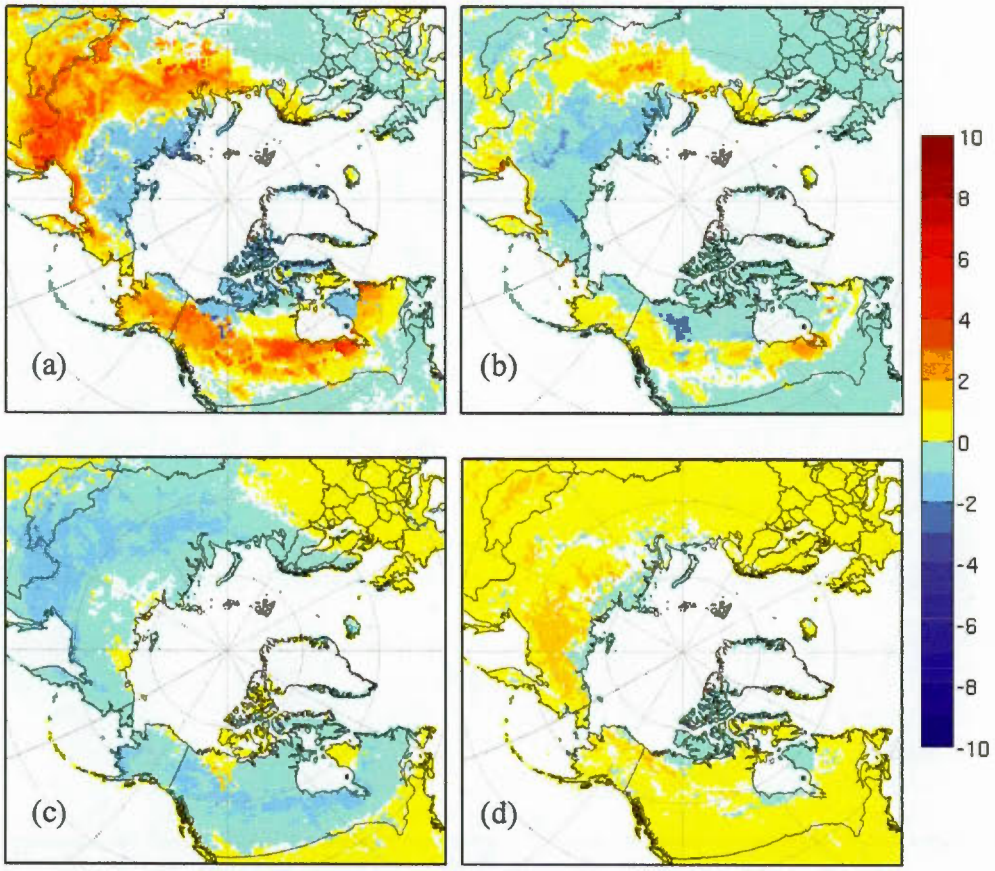

Figure A.1 (a) Difference (CLASS26_CTEM/ERA - CLASS3_CTEM/ERA) in 1981-2010 winter (DJF) temperature [K] of the first soil layer. (b) Same, but for spring (MAM). (c) Same, but for summer (JJA). (d) Same, but for fall (SON).

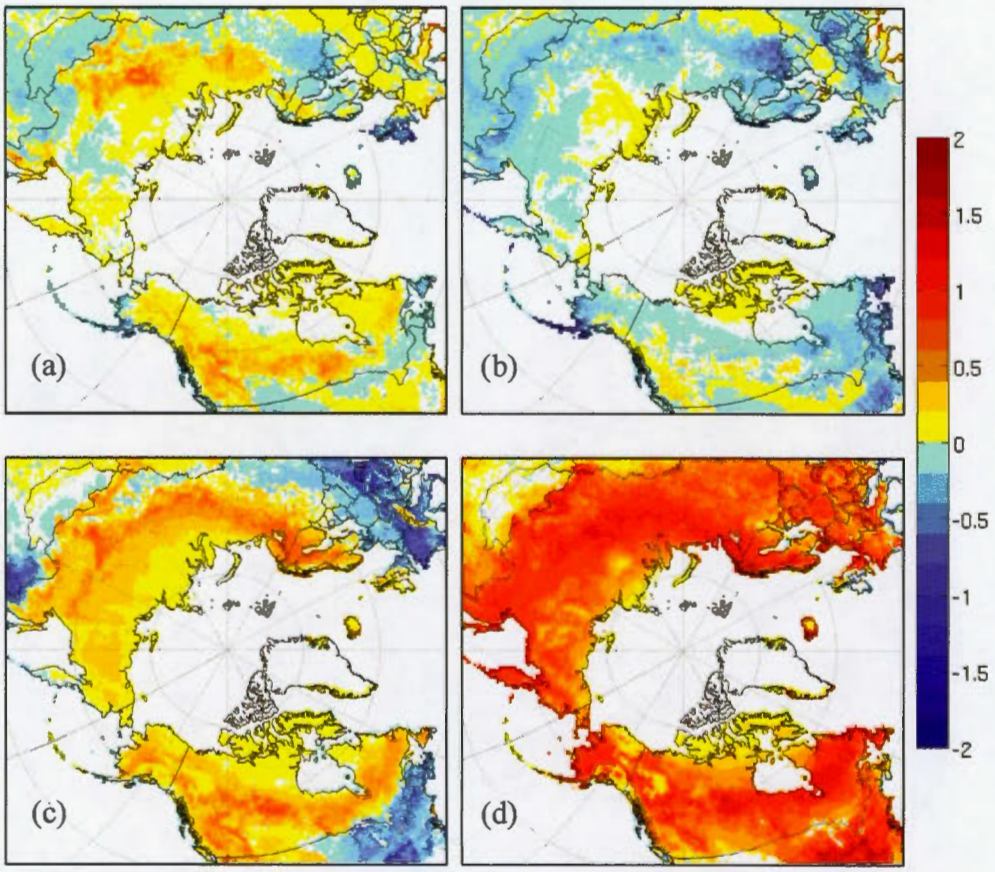

Figure A.2 (a) Difference (CLASS26_CTEM/ERA - CLASS26/ERA) in 1981-2010 winter (DJF) PAI [m^2 m^{-2}]. (b) Same, but for spring (MAM). (c) Same, but for summer (JJA). (d) Same, but for fall (SON).

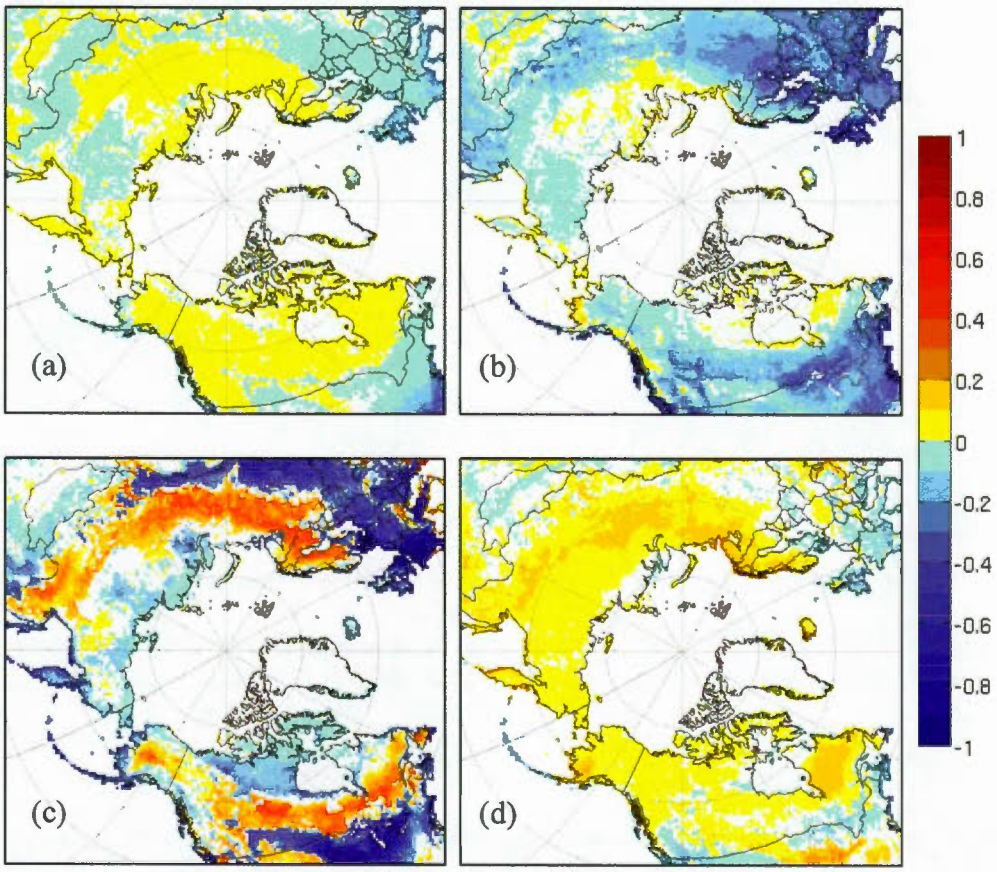

Figure A.3 (a) Difference (CLASS26_CTEM/ERA - CLASS26/ERA) in 1981-2010 winter (DJF) evapotranspiration [mm day^{-1}]. (b) Same, but for spring (MAM). (c) Same, but for summer (JJA). (d) Same, but for fall (SON).

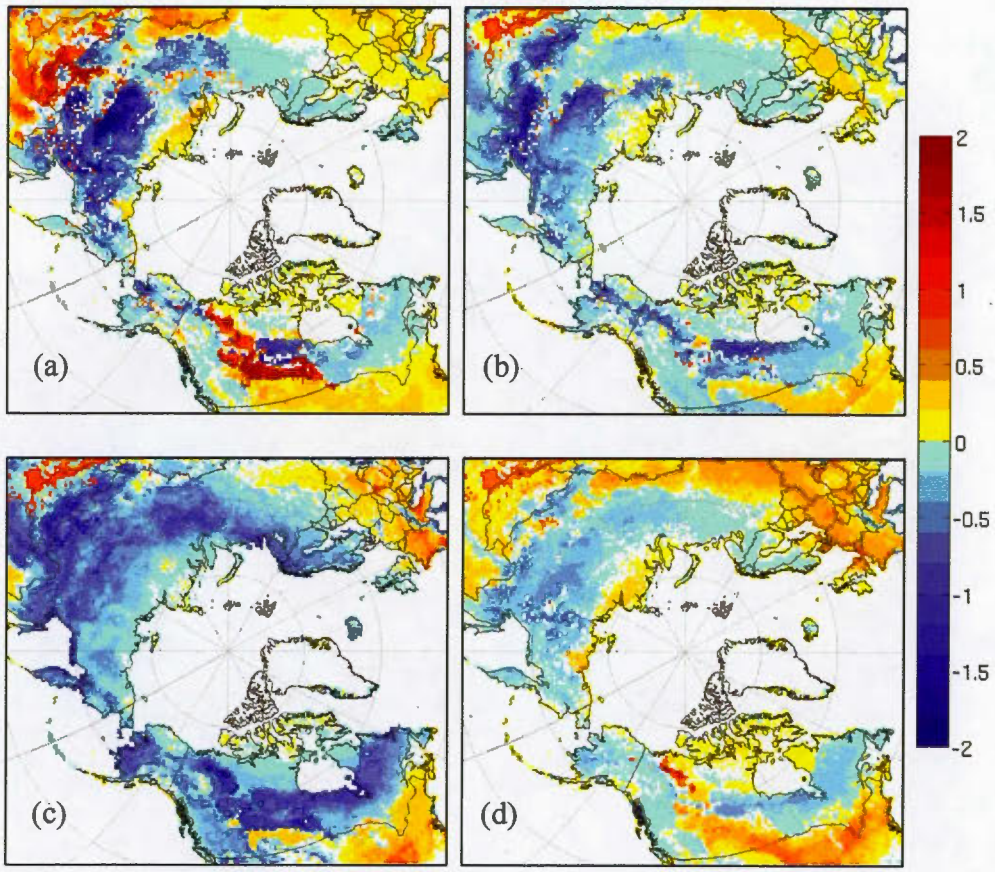

Figure A.4 (a) Difference (CLASS26_CTEM/ERA - CLASS26/ERA) in 1981-2010 winter (DJF) temperature [K] of the first soil layer. (b) Same, but for spring (MAM). (c) Same, but for summer (JJA). (d) Same, but for fall (SON).

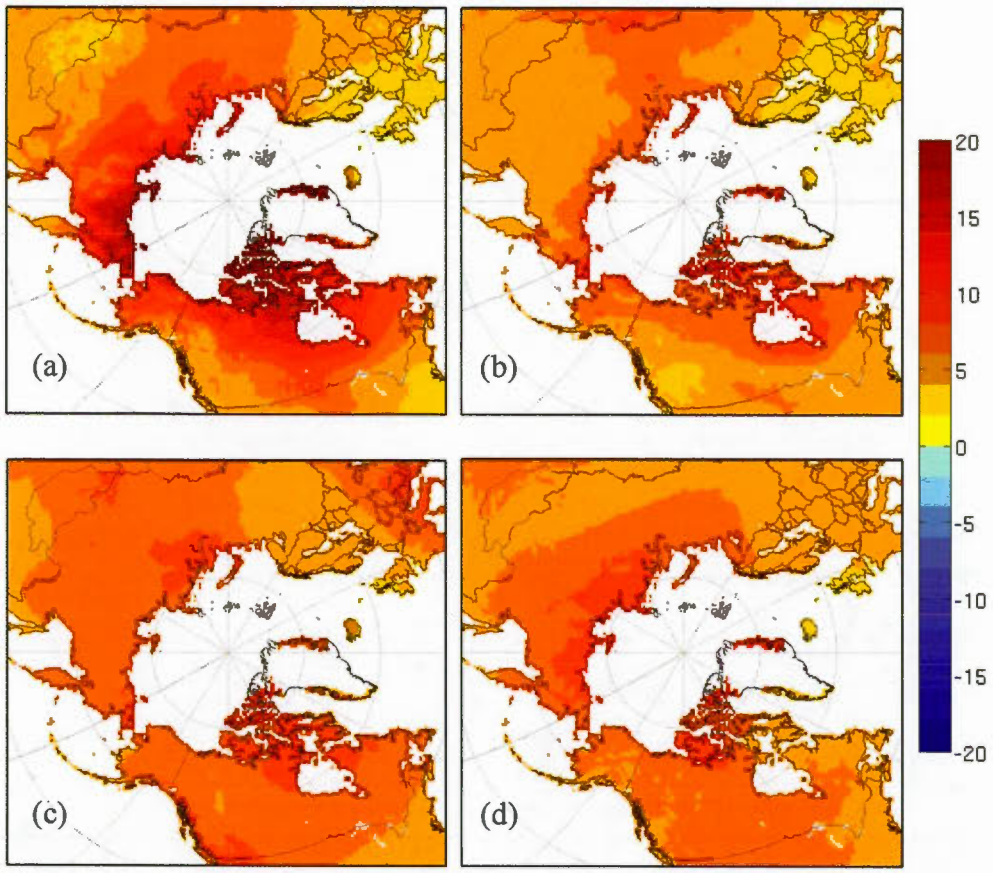

Figure A.5 (a) Projected changes (2071-2100 minus 1981-2010) in winter (DJF) driving air temperature [K]. (b) Same, but for spring (MAM). (c) Same, but for summer (JJA). (d) Same, but for fall (SON).

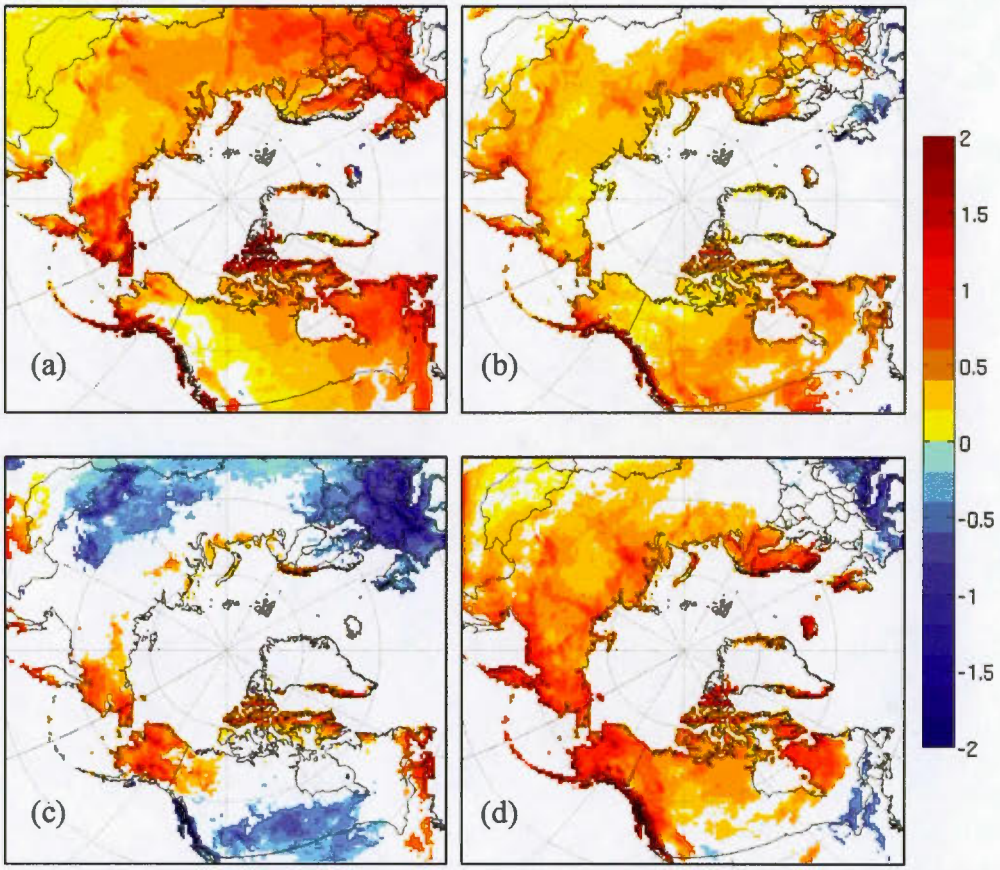

Figure A.6 (a) Projected changes (2071-2100 minus 1981-2010) in winter (DJF) driving precipitation [mm day^{-1}]. (b) Same, but for spring (MAM). (c) Same, but for summer (JJA). (d) Same, but for fall (SON).

REFERENCES

Arnell, N.W. (2005). Implications of climate change for freshwater inflows to the Arctic Ocean. *Journal of Geophysical Research-Atmospheres, 110*(D7).

Arora, V.K. (2003). Simulating energy and carbon fluxes over winter wheat using coupled land surface and terrestrial ecosystem models. *Agricultural and Forest Meteorology, 118*(1-2), 21-47.

Arora, V.K. and Boer, G.J. (2003). A Representation of Variable Root Distribution in Dynamic Vegetation Models. *Earth Interactions, 7*.

Arora, V.K. and Boer, G.J. (2005). A parameterization of leaf phenology for the terrestrial ecosystem component of climate models. *Global Change Biology, 11*(1), 39-59.

Arora, V.K. and Boer, G.J. (2006). Simulating competition and coexistence between plant functional types in a dynamic vegetation model. *Earth Interactions, 10*.

Betts, R.A., Cox, P.M., Lee, S.E. and Woodward, F.I. (1997). Contrasting physiological and structural vegetation feedbacks in climate change simulations. *Nature, 387*(6635), 796-799.

Brown, J., Ferrians Jr, O.J., Heginbottom, J.A. and Melnikov, E.S. (1997). *Circum-Arctic map of permafrost and ground-ice conditions*. [Report].

Brown, J., Hinkel, K.M. and Nelson, F.E. (2000). The circumpolar active layer monitoring (calm) program: Research designs and initial results. *Polar Geography, 24*(3), 166-258.

Carroll, M., Townshend, J., Hansen, M., DiMiceli, C., Sohlberg, R. and Wurster, K. (2011). MODIS Vegetative Cover Conversion and Vegetation Continuous Fields. Dans *Land Remote Sensing and Global Environmental Change* (p. 725-745): Springer.

Cramer, W., Bondeau, A., Woodward, F.I., Prentice, I.C., Betts, R.A., Brovkin, V., Cox, P.M., Fisher, V., Foley, J.A., Friend, A.D., Kucharik, C., Lomas, M.R., Ramankutty, N., Sitch, S., Smith, B., White, A. and Young-Molling, C. (2001). Global response of terrestrial ecosystem structure and function to CO2 and climate change: results from six dynamic global vegetation models. *Global Change Biology, 7*(4), 357-373.

Dee, D.P., Uppala, S.M., Simmons, A.J., Berrisford, P., Poli, P., Kobayashi, S., Andrae, U., Balmaseda, M.A., Balsamo, G., Bauer, P., Bechtold, P., Beljaars, A.C.M., van de Berg, L., Bidlot, J., Bormann, N., Delsol, C., Dragani, R., Fuentes, M., Geer, A.J., Haimberger, L., Healy, S.B., Hersbach, H., Holm, E.V., Isaksen, L., Kallberg, P., Kohler, M., Matricardi, M., McNally, A.P., Monge-Sanz, B.M., Morcrette, J.J., Park, B.K., Peubey, C., de Rosnay, P., Tavolato, C., Thepaut, J.N. and Vitart, F. (2011). The ERA-Interim reanalysis: configuration and performance of the data assimilation system. *Quarterly Journal of the Royal Meteorological Society, 137*(656), 553-597.

Delisle, G. (2007). Near-surface permafrost degradation: How severe during the 21st century? *Geophysical Research Letters, 34*(9).

Di Luca, A., de Elía, R. and Laprise, R. (2012). Potential for added value in temperature simulated by high-resolution nested RCMs in present climate and in the climate change signal. *Climate Dynamics, 40*(1-2), 443-464.

FAO. (1995). *Digital Soil Map of the World* Rome, Italy: FAO.

Farquhar, G.D., von Caemmerer, S. and Berry, J.A. (1980). A biochemical model of photosynthetic CO2 assimilation in leaves of C 3 species. *Planta, 149*(1), 78-90.

Feser, F., Rockel, B., von Storch, H., Winterfeldt, J. and Zahn, M. (2011). REGIONAL CLIMATE MODELS ADD VALUE TO GLOBAL MODEL DATA A Review and Selected Examples. *Bulletin of the American Meteorological Society, 92*(9), 1181-1192.

Field, C.B., Jackson, R.B. and Mooney, H.A. (1995). Stomatal Responses to Increased CO2 - Implications from the Plant to the Global-Scale. *Plant Cell and Environment, 18*(10), 1214-1225.

Friedl, M.A., Sulla-Menashe, D., Tan, B., Schneider, A., Ramankutty, N., Sibley, A. and Huang, X.M. (2010). MODIS Collection 5 global land cover: Algorithm refinements and characterization of new datasets. *Remote Sensing of Environment, 114*(1), 168-182.

Garnaud, C., Sushama, L. and Arora, V.K. (2014a). The effect of driving climate data on the simulated terrestrial carbon pools and fluxes over North America. *International Journal of Climatology, 34*(4), 1098-1110.

Garnaud, C., Sushama, L. and Verseghy, D. (2014b). Impact of interactive vegetation phenology on the Canadian RCM simulated climate over North America. *Climate Dynamics, 45*(5-6), 1471-1492.

Hugelius, G., Tarnocai, C., Broll, G., Canadell, J.G., Kuhry, P. and Swanson, D.K. (2013). The Northern Circumpolar Soil Carbon Database: spatially distributed datasets of soil coverage and soil carbon storage in the northern permafrost regions. *Earth System Science Data, 5*(1), 3-13.

IPCC. (2013). *Climate Change 2013: The Physical Science Basis. Contribution of Working Group I to the Fifth Assessment Report of the Intergovernmental Panel on Climate Change*. Cambridge, United Kingdom and New York, NY, USA: Cambridge University Press.

Kaufman, D.S., Schneider, D.P., McKay, N.P., Ammann, C.M., Bradley, R.S., Briffa, K.R., Miller, G.H., Otto-Bliesner, B.L., Overpeck, J.T. and Vinther, B.M. (2009). Recent warming reverses long-term arctic cooling. [Research Support, U.S. Gov't, Non-P.H.S.]. *Science, 325*(5945), 1236-1239.

Koven, C.D., Riley, W.J. and Stern, A. (2013). Analysis of Permafrost Thermal Dynamics and Response to Climate Change in the CMIP5 Earth System Models. *Journal of Climate, 26*(6), 1877-1900.

Laprise, R. (2008). Regional climate modelling. *Journal of Computational Physics, 227*(7), 3641-3666.

Lawrence, D.M. and Slater, A.G. (2005). A projection of severe near-surface permafrost degradation during the 21st century. *Geophysical Research Letters, 32*(24).

Letts, M.G., Roulet, N.T., Comer, N.T., Skarupa, M.R. and Verseghy, D.L. (2000). Parametrization of peatland hydraulic properties for the Canadian Land Surface Scheme. *Atmosphere-Ocean, 38*(1), 141-160.

Liu, Z.Y., Notaro, M., Kutzbach, J. and Liu, N. (2006). Assessing global vegetation-climate feedbacks from observations. *Journal of Climate, 19*(5), 787-814.

Meinshausen, M., Smith, S.J., Calvin, K., Daniel, J.S., Kainuma, M.L.T., Lamarque, J.F., Matsumoto, K., Montzka, S.A., Raper, S.C.B., Riahi, K., Thomson, A., Velders, G.J.M. and van Vuuren, D.P.P. (2011). The RCP greenhouse gas concentrations and their extensions from 1765 to 2300. *Climatic Change, 109*(1-2), 213-241.

Murray-Tortarolo, G., Anav, A., Friedlingstein, P., Sitch, S., Piao, S.L., Zhu, Z.C., Poulter, B., Zaehle, S., Ahlstrom, A., Lomas, M., Levis, S., Viovy, N. and Zeng, N. (2013). Evaluation of Land Surface Models in Reproducing Satellite-Derived LAI over the High-Latitude Northern Hemisphere. Part I: Uncoupled DGVMs. *Remote Sensing, 5*(10), 4819-4838.

Nemani, R.R., Keeling, C.D., Hashimoto, H., Jolly, W.M., Piper, S.C., Tucker, C.J., Myneni, R.B. and Running, S.W. (2003). Climate-driven increases in global terrestrial net primary production from 1982 to 1999. [Research Support, U.S. Gov't, Non-P.H.S.]. *Science, 300*(5625), 1560-1563.

Paquin, J.P. and Sushama, L. (2014). On the Arctic near-surface permafrost and climate sensitivities to soil and snow model formulations in climate models. *Climate Dynamics, 44*(1-2), 203-228.

Pearson, R.G., Phillips, S.J., Loranty, M.M., Beck, P.S.A., Damoulas, T., Knight, S.J. and Goetz, S.J. (2013). Shifts in Arctic vegetation and associated feedbacks under climate change. *Nature Climate Change, 3*(7), 673-677.

Pribyl, D.W. (2010). A critical review of the conventional SOC to SOM conversion factor. *Geoderma, 156*(3-4), 75-83.

Quillet, A., Peng, C.H. and Garneau, M. (2010). Toward dynamic global vegetation models for simulating vegetation-climate interactions and feedbacks: recent developments, limitations, and future challenges. *Environmental Reviews, 18*, 333-353.

Raich, J.W. and Schlesinger, W.H. (1992). The Global Carbon-Dioxide Flux in Soil Respiration and Its Relationship to Vegetation and Climate. *Tellus Series B-Chemical and Physical Meteorology, 44*(2), 81-99.

Richardson, A.D., Keenan, T.F., Migliavacca, M., Ryu, Y., Sonnentag, O. and Toomey, M. (2013). Climate change, phenology, and phenological control of vegetation feedbacks to the climate system. *Agricultural and Forest Meteorology, 169*, 156-173.

Schuur, E.A., McGuire, A.D., Schadel, C., Grosse, G., Harden, J.W., Hayes, D.J., Hugelius, G., Koven, C.D., Kuhry, P., Lawrence, D.M., Natali, S.M., Olefeldt, D., Romanovsky, V.E., Schaefer, K., Turetsky, M.R., Treat, C.C. and Vonk, J.E. (2015). Climate change and the permafrost carbon feedback. *Nature, 520*(7546), 171-179.

Schuur, E.A.G., Abbott, B.W., Bowden, W.B., Brovkin, V., Camill, P., Canadell, J.G., Chanton, J.P., Chapin, F.S., Christensen, T.R., Ciais, P., Crosby, B.T., Czimczik, C.I., Grosse, G., Harden, J., Hayes, D.J., Hugelius, G., Jastrow, J.D., Jones, J.B., Kleinen, T., Koven, C.D., Krinner, G., Kuhry, P., Lawrence, D.M., McGuire, A.D., Natali, S.M., O'Donnell, J.A., Ping, C.L., Riley, W.J.,

Rinke, A., Romanovsky, V.E., Sannel, A.B.K., Schadel, C., Schaefer, K., Sky, J., Subin, Z.M., Tarnocai, C., Turetsky, M.R., Waldrop, M.P., Anthony, K.M.W., Wickland, K.P., Wilson, C.J. and Zimov, S.A. (2013). Expert assessment of vulnerability of permafrost carbon to climate change. *Climatic Change, 119*(2), 359-374.

Serreze, M.C. and Barry, R.G. (2011). Processes and impacts of Arctic amplification: A research synthesis. *Global and Planetary Change, 77*(1-2), 85-96.

Sietse, O. (2010). ISLSCP II FASIR-adjusted NDVI, 1982-1998. *ISLSCP Initiative II Collection. Data set. Available on-line [*http://daac. *ornl. gov/] from Oak Ridge National Laboratory Distributed Active Archive Center, Oak Ridge, Tennessee, USA doi, 10.*

Slater, A.G. and Lawrence, D.M. (2013). Diagnosing Present and Future Permafrost from Climate Models. *Journal of Climate, 26*(15), 5608-5623.

Smith, L.C., Pavelsky, T.M., MacDonald, G.M., Shiklomanov, A.I. and Lammers, R.B. (2007). Rising minimum daily flows in northern Eurasian rivers: A growing influence of groundwater in the high-latitude hydrologic cycle. *Journal of Geophysical Research-Biogeosciences, 112*(G4).

Smith, L.C., Sheng, Y., MacDonald, G.M. and Hinzman, L.D. (2005). Disappearing Arctic lakes. *Science, 308*(5727), 1429.

St. Jacques, J.-M. and Sauchyn, D.J. (2009). Increasing winter baseflow and mean annual streamflow from possible permafrost thawing in the Northwest Territories, Canada. *Geophysical Research Letters, 36*(1).

Stephenson, N.L. (1990). Climatic Control of Vegetation Distribution - the Role of the Water-Balance. *American Naturalist, 135*(5), 649-670.

Swann, A.L., Fung, I.Y., Levis, S., Bonan, G.B. and Doney, S.C. (2010). Changes in Arctic vegetation amplify high-latitude warming through the greenhouse effect. *Proceedings of the National Academy of Sciences of the United States of America, 107*(4), 1295-1300.

Tarnocai, C., Canadell, J.G., Schuur, E.A.G., Kuhry, P., Mazhitova, G. and Zimov, S. (2009). Soil organic carbon pools in the northern circumpolar permafrost region. *Global Biogeochemical Cycles, 23*(2).

Task, G.S.D. (2000). Global Soil Data Products CD-ROM (IGBP-DIS). *International Geosphere-Biosphere Programme-Data and Information Available Services [Available online at* http://www. *daac. ornl. gov].*

Turetsky, M.R., Kane, E.S., Harden, J.W., Ottmar, R.D., Manies, K.L., Hoy, E. and Kasischke, E.S. (2010). Recent acceleration of biomass burning and carbon losses in Alaskan forests and peatlands. *Nature Geoscience, 4*(1), 27-31.

Verseghy, D.L. (1991). Class-a Canadian Land Surface Scheme for Gcms .1. Soil Model. *International Journal of Climatology, 11*(2), 111-133.

Verseghy, D.L., Mcfarlane, N.A. and Lazare, M. (1993). Class - a Canadian Land-Surface Scheme for Gcms .2. Vegetation Model and Coupled Runs. *International Journal of Climatology, 13*(4), 347-370.

Webb, R.S., Rosenzweig, C.E. and Levine, E.R. (1993). Specifying Land Surface Characteristics in General-Circulation Models - Soil-Profile Data Set and Derived Water-Holding Capacities. *Global Biogeochemical Cycles, 7*(1), 97-108.

Wramneby, A., Smith, B. and Samuelsson, P. (2010). Hot spots of vegetation-climate feedbacks under future greenhouse forcing in Europe. *Journal of Geophysical Research-Atmospheres, 115*(D21).

Xu, L., Myneni, R.B., Chapin, F.S., Callaghan, T.V., Pinzon, J.E., Tucker, C.J., Zhu, Z., Bi, J., Ciais, P., Tommervik, H., Euskirchen, E.S., Forbes, B.C., Piao, S.L., Anderson, B.T., Ganguly, S., Nemani, R.R., Goetz, S.J., Beck, P.S.A., Bunn, A.G., Cao, C. and Stroeve, J.C. (2013). Temperature and vegetation seasonality diminishment over northern lands. *Nature Climate Change, 3*(6), 581-586.

Zhang, T., Barry, R.G., Knowles, K., Heginbottom, J.A. and Brown, J. (2008). Statistics and characteristics of permafrost and ground-ice distribution in the Northern Hemisphere. *Polar Geography, 31*(1-2), 47-68.

Zhang, W., Jansson, C., Miller, P.A., Smith, B. and Samuelsson, P. (2014). Biogeophysical feedbacks enhance the Arctic terrestrial carbon sink in regional Earth system dynamics. *Biogeosciences, 11*(19), 5503-5519.

Zhao, M.S., Heinsch, F.A., Nemani, R.R. and Running, S.W. (2005). Improvements of the MODIS terrestrial gross and net primary production global data set. *Remote Sensing of Environment, 95*(2), 164-176.